Electronic Supplementary Information 1

Acylthioureas as anion transporters: the effect of intramolecular hydrogen bonding

Cally J. E. Haynes,[a] Nathalie Busschaert,[a] Isabelle L. Kirby,[a] Julie Herniman,[a] Mark E. Light,[a] Neil J. Wells,[a] Igor Marques,[b] Vítor Félix[b] and Philip A. Gale*[a]

Contents

1 General Remarks

^{1}H NMR (300 MHz), ^{19}F NMR (282 MHz) and ^{13}C{1H} NMR (75 MHz) spectra were determined on a Bruker spectrometer. ^{1}H NMR (400 MHz) and ^{13}C{1H} NMR (100 MHz) spectra were determined on a Bruker DPX400 spectrometer. COSY NMR spectra were determined on a Bruker AVII400 spectrometer. Chemical shifts (**δ**) are reported in parts per million (ppm) and calibrated to the residual solvent peak in DMSO-d_6 (δ = 2.50 (^{1}H) and 39.51 ppm (^{13}C)). The following abbreviations are used for spin multiplicity: s = singlet, d = doublet, dd = doublet of doublets, t = triplet, q = quartet, m = multiplet, br = broad. Infrared (IR) spectra were recorded on a Matterson Satellite (ATR) and are reported in wavenumbers (cm-1). High resolution electron spray (ES) mass spectra were recorded on a Bruker maXis ESI. All mass spectra are reported as *m/z* (relative intensity). Melting points were determined by a Barnstead Electrothermal 9100 melting point apparatus and were not corrected. Chloride concentrations during transport experiments were determined using an Accumet chloride-selective electrode. POPC (1-palmitoyl-2-oleoyl-sn-glycero-3- phosphocholine) was supplied by Corden-Pharma and was stored at –20°C as a solution in chloroform (1 g POPC in 35 mL chloroform). Polyoxyethylene(8)lauryl ether was used as detergent (TCI).

2 Synthesis

N-(hexylcarbamothioyl)benzamide 5

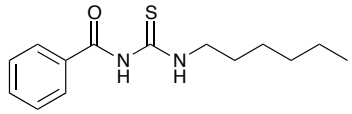

Benzoyl isothiocyanate (0.20 g, 1.23 mmol) and hexylamine (0.123 g, 1.23 mmol) were dissolved in 1 mL ethyl acetate and stirred for 30 minutes. The solvent was removed under reduced pressure and the crude product was purified by column chromatography on silica (DCM) to give **5** as a colourless oil.

Yield: 0.285 g (88 %); **^{1}H NMR** (300 MHz, DMSO-*d*$_6$) δ = 11.27 (s, 1H, NH), 10.88 (t, *J* = 4.9 Hz, NH), 7.92 (m, 2H, Ar-CH), 7.63 (m, 1H, Ar-CH), 7.51 (m, 2H, Ar-CH), 3.60 (m, 2H, CH_2), 1.61 (m, 2H, CH_2), 1.33 (m, 6H, 3 x CH_2), 0.87 (m, 3H, CH_3); **^{13}C NMR** (75 MHz, DMSO-*d*$_6$): δ= 180.0 (C=S), 168.0 (C=O), 132.9, 132.2 128.5, 44.7, 30.9, 27.5, 26.0, 22.0, 13.9; **LRMS (ESI+)** *m/z*: 264.1 $[M + H]^+$; **HRMS (ES+)** *m/z*: $[M + H]^+$ calculated 265.1375, found 265.1366; $[M + Na]^+$ calculated 287.1194, found 287.1188. **IR (film)**: ν= 3210, 2930, 2850, 1670 (C=O stretching), 1510 (C=S stretching).

Acyl thiourea synthesis: general procedure

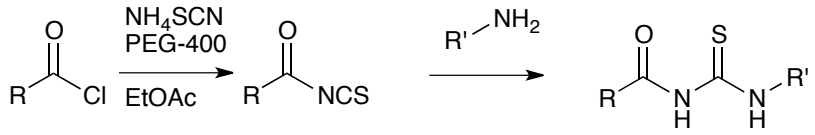

The acid chloride (5.5 mmol) was dissolved in 7.5 mL ethyl acetate and ammonium thiocyanate (0.494 g, 6.5 mmol) and PEG-400 (0.08 g) were added. The reaction was stirred for 1 h, after which an amine (5.5 mmol) was added and the reaction was stirred for a further 30 min. The inorganic solids were removed by filtration and the crude product (filtrate) was purified by column chromatography on silica (eluents detailed below).

N-(hexylcarbamothioyl)-4-(trifluoromethyl)benzamide 6

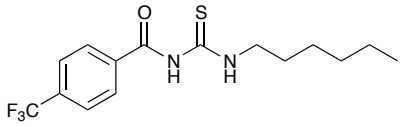

Purified by column chromatography on silica (DCM) to give the product as a white crystalline solid.

Yield: 0.600 g (33 %); **^{1}H NMR** (300 MHz, DMSO-*d6*) δ = 11.56 (s, 1H, NH), 10.78 (t, *J* = 5.1 Hz, 1H, NH), 8.09 (d, *J* = 8.1 Hz, 2H, Ar-CH), 7.87 (d, *J* = 8.4 Hz, 2H, Ar-CH), 3.61 (m, 2H, CH_2), 1.61 (m, 2H, CH_2), 1.33 (m, 6H, 3 x CH_2), 0.87 (t, *J* = 6.6 Hz, 3H, CH_3); **^{19}F NMR** (300 MHz, DMSO-*d6*) 61.28 (CF_3); **^{13}C NMR** (75 MHz, DMSO-*d6*): δ= 179.7 (C=S), 167.0 (C=O), 136.3, 132.3 (q, J_{C-F} = 32.1 Hz, *C*-CF_3), 129.5, 125.3, 123.8 (q, J_{C-F} = 272.6 Hz, CF_3), 121.9, 118.3, 44.8, 30.9, 27.5, 26.1, 22.0; **Mp**: 58-60 °C; **LRMS (ESI+)** *m/z*: 333.2 $[M + H]^+$, 355.3 $[M + Na]^+$; **HRMS (ES+)** *m/z*: $[M + H]^+$ calculated 333.1248, found 333.1229. **IR (film)**: ν=3210, 2930, 2850, 1670 (carbonyl C=O stretching), 1534 (C=S stretching).

N-(hexylcarbamothioyl)-4-methoxybenzamide 7

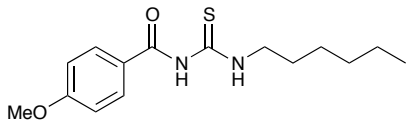

Purified by column chromatography on silica (DCM) to give the product as a colourless oil which formed a white crystalline solid on scratching.

Yield: 0.820 g (51 %); **^{1}H NMR** (300 MHz, DMSO-*d6*) δ = 11.07 (s, 1H, NH), 10.95 (t, *J* = 5.1 Hz, 1H, NH), 7.96 (d, *J* = 8.8 Hz, 2H, Ar-CH), 7.03 (d, *J* = 9.1 Hz, 2H, Ar-CH), 3.84 (s, 3H, OCH_3), 3.59 (m, 2H, CH_2), 1.60 (m, 2H, CH_2), 1.29 (m, 6H, 3 x CH_2), 0.87 (t, *J* = 6.6 Hz, CH_3); **^{13}C NMR** (75 MHz, DMSO-*d6*): δ= 180.1 (C=S), 167.3 (C=O), 163.1, 130.8, 124.0, 113.7, 55.6, 44.7, 30.9, 27.5, 26.0, 22.0, 13.9; **Mp**: 62-64 °C; **LRMS (ESI+)** *m/z*: 295.3 $[M + H]^+$, 317.3 $[M + Na]^+$; **HRMS (ES+)** *m/z*: $[M + H]^+$ calculated 295.1480, found 295.1472; $[M + Na]^+$ calculated 317.1300, found 317.1294; **IR (film)**: ν = 3340, 3210, 2960, 2930, 2850, 1650 (C=O stretching), 1600.

N-(hexylcarbamothioyl)-4-pentylbenzamide 8

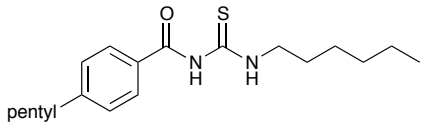

Purified by column chromatography on silica (DCM/ hexane 1:1) to give the product as a colourless oil.

Yield: 0.945 g (51 %); **^{1}H NMR** (300 MHz, DMSO-*d6*) δ = 11.14 (s, 1H, NH), 10.92 (t, *J* = 5.3 Hz, 1H, NH), 7.86 (d, *J* = 8.4 Hz, 2H, Ar-CH), 7.32 (d, *J* = 8.4 Hz, 2H, Ar-CH), 3.59 (m, 2H, CH_2), 2.63 (t, *J* = 7.7 Hz, 2H, aromatic adjascent CH_2), 1.48 (m, 4H, 2 x CH_2), 1.29 (m, 10H, 5 x CH_2), 0.86 (m, 6H, 2 x CH_3); **^{13}C NMR** (75 MHz, DMSO-*d6*): δ= 180.0 (C=S), 167.8 (C=O), 148.0, 129.6, 128.6, 128.3, 44.7, 35.0, 30.9, 30.2, 27.5, 26.0, 22.0, 21.9, 13.9 (alkyl resonances overlapping); **LRMS (ESI+)** *m/z*: 335.1 $[M + H]^+$, 358.2 $[M + Na]^+$; **HRMS (ES+)** *m/z*: $[M + NH]^+$ calculated 335.2157, found 335.2150; $[M + Na]^+$ calculated 357.1977, found 357.1971; **IR (film)**: ν=3250, 2920, 2850, 1670 (C=O stretching), 1570.

N-(dipropylcarbamothioyl)benzamide 9

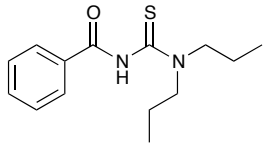

Benzoyl isothiocyanate (0.500 g, 5.5 mmol) was dissolved in 7 mL EtOAc and dipropylamine (0.310 g, 5.5 mmol) was added. The reaction was stirred at room temperature for 1 hour, after which the crude product was purified by column chromatography on silica (DCM) to give **9** as an off-white waxy solid. **In the characterizing NMR spectra, the two propyl groups were found to be inequivalent.**

Yield: 0.650 g, 45 %; **^{1}H NMR** (300 MHz, DMSO-*d*$_6$): δ= 10.58 (br. s, 1H, NH), 7.91 (m, 2H, Ar-CH), 7.60 (m, 1H, Ar-CH), 7.50 (m, 2H, Ar-CH), 3.88 (t, *J* = 7.3 Hz, 2H, CH_2), 3.42 (t, *J* = 7.5 Hz, 2H, CH_2), 1.75 (m, 2H, CH_2), 1.63 (m, 2H, CH_2), 0.94 (t, *J* = 7.3 Hz, 3H, CH_3), 0.80 (t, *J* = 7.3 Hz, 3H, CH_3); **^{13}C NMR** (75 MHz, DMSO-*d*$_6$): δ= 181.5 (C=S), 163.8 (C=O), 133.0, 132.2, 128.4, 128.0, 54.3, 53,7, 21.2, 19.1, 11.1; **Mp**: 64-67 °C **LRMS (ESI+)** *m/z*: 265.2 $[M + H]^+$, 287.1 $[M + Na]^+$; **HRMS (ES+)** *m/z*: $[M + H]^+$ calculated 265.1375, found 265.1369; $[M + Na]^+$ calculated 287.1194, found 287.1192. **IR (film)**: ν=3140, 2960, 2930, 2870, 1670 (C=O stretching), 1540.

N-(hexylcarbamoyl)benzamide 10

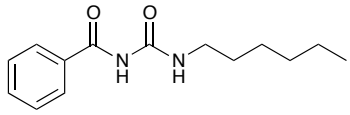

Benzoyl isocyanate (0.200 g, 1.35 mmol) was dissolved in 5 mL EtOAc and hexylamine (0.138 g, 1.35 mmol) was added. The reaction was stirred at room temperature for 1 hour and monitored by TLC. After 1 hour, the solvent was removed and the crude product was purified by column chromatography on silica (DCM) to give **10** as a white crystalline solid.

Yield: 0.100 g, 30 %; **^{1}H NMR** (300 MHz, DMSO-*d*$_6$) δ = 10.65 (s, 1H, NH), 8.66 (t, *J* = 5.5 Hz, 1H, NH), 7.96 (m, 2H, Ar-CH), 7.61 (m, 1H, Ar-CH), 7.49 (m, 2H, Ar-CH), 3.22 (q, *J* = 6.6 Hz, 2H, CH_2), 1.49 (m, 2H, CH_2), 1.30 (m, 6H, 3 x CH_2), 0.87 (t, *J* = 6.59 Hz,

3H, CH_3);

^{13}C NMR (75 MHz, DMSO-*d*$_6$): δ= 168.2 (C=O), 153.5 (C=O), 132.7, 128.4, 128.1, (1 alkyl C resonance underneath DMSO), 30.9, 29.1, 26.0, 22.0, 13.9; **Mp**: 88-90 °C **LRMS (ESI+)** *m/z*: 265.2 $[M + H]^+$, 287.1 $[M + Na]^+$; **HRMS (ES+)** *m/z*: $[M + H]^+$ calculated 249.1603, found 249.1593; $[M + Na]^+$ calculated 271.1422, found 271.1417; **IR (film)**: ν=3310, 2920, 2850, 1690 (C=O stretching), 1660 (C=O stretching).

N-(hexylcarbamoyl)benzothioamide 11

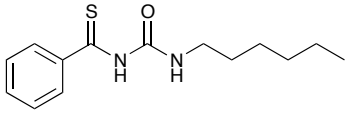

Thiobenzamide (0.500 g, 3.64 mmol) was dissolved in 10 mL MeCN and KOH (~200 mg, pellets) was added. The solution was stirred for 20 min, after which hexyl isothiocyanate (0.463 g, 3.64 mmol) was added. The reaction was stirred for a further 30 min, then diluted with 100 mL water and extracted with DCM. The organic phase was dried over $MgSO_4$ and purified by column chromatography on silica (DCM/ hexane 3:1) to give the product as a yellow oil which formed a crystalline solid on standing.

Yield: 0.670 g (70 %); **^{1}H NMR** (300 MHz, DMSO-*d*$_6$) δ = 11.74 (s, 1H, NH), 9.26 (br. s, 1H, NH), 7.67 (m, 2H, Ar-CH), 7.52 (m, 1H, Ar-CH), 7.41 (m, 2H, Ar-CH), 3.24 (m, 2H, CH_2), 1.50 (m, 2H, CH_2), 1.31 (m, 6H, 3 x CH_2), 0.87 (t, *J* = 6.59 Hz, 3H, CH_3); **^{13}C NMR** (75 MHz, DMSO-*d*$_6$): δ= 153.0 (C=S), 141.9 (C=O), 131.4, 127.9, 127.5, (1 alkyl C under DMSO peak), 30.8, 28.7, 26.0, 22.0. 13.9; **Mp**: 48-50 °C **LRMS (ESI+)** *m/z*: 265.2 $[M + H]^+$, 287.1 $[M + Na]^+$; **HRMS (ES+)** *m/z*: $[M + H]^+$ calculated 265.1375, found 265.1366; $[M + Na]^+$ calculated 287.1194, found 287.1193; **IR (film)**: ν= 3110, 3030, 2930, 2920, 2850, 1690 (C=O stretching), 1550.

N-(hexylcarbamothioyl)benzothioamide 12

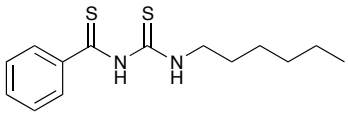

Thiobenzamide (0.500 g, 3.64 mmol) was dissolved in 10 mL MeCN and KOH (~200 mg, pellets) was added. The solution was stirred for 20 min, after which hexyl isocyanate

(0.521 g, 3.64 mmol) was added. The reaction was stirred for a further 30 min, then diluted with 100 mL water and extracted with DCM. The organic phase was dried over $MgSO_4$ and purified by column chromatography on silica (DCM/ hexane 9:1) followed by preparatory TLC (DCM/ hexane 75:25) to give a viscous orange oil which formed a solid when under vacuum. The product was found to decompose during the purification process and therefore was not isolated cleanly (a ^1H NMR spectrum can be seen below). The product was found to further degrade over time to give a strong smell of hydrogen sulfide accompanied by a blackening of the oil and the growth of crystals of elemental sulfur (S_8).

3 NMR Spectra (recorded in DMSO-d_6)

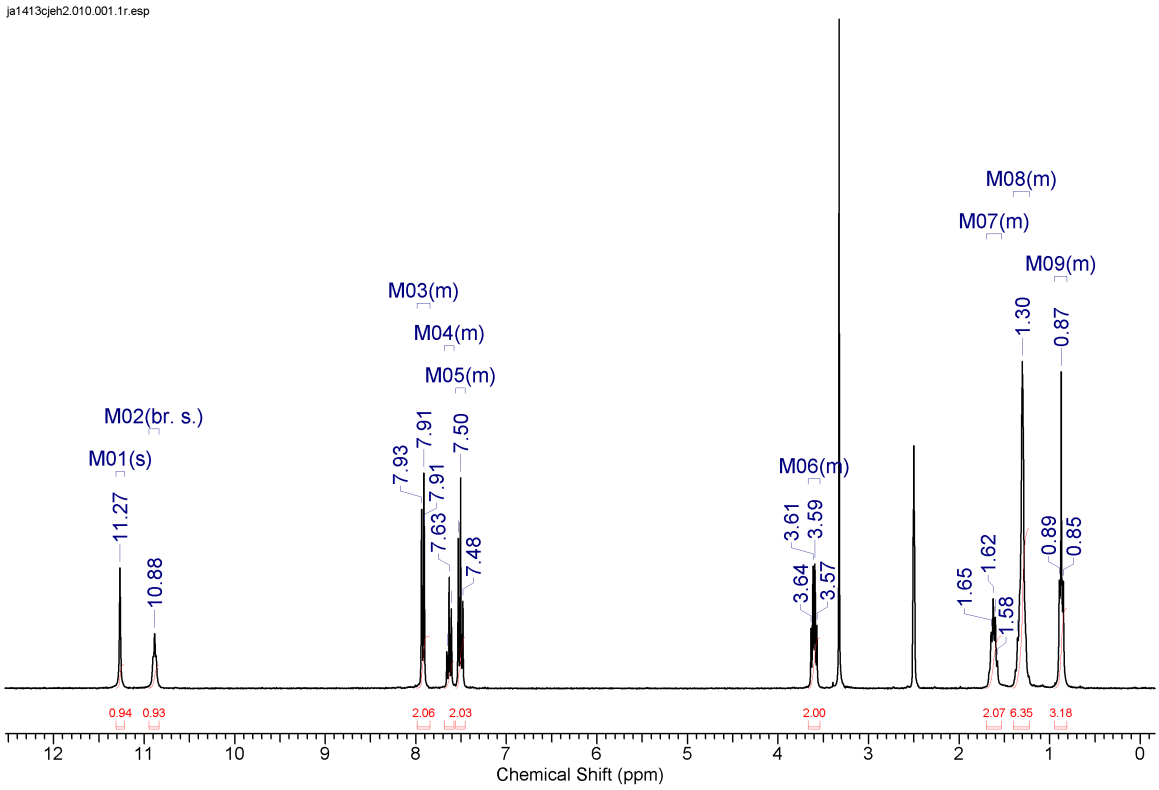

Fig. S1 The ^{1}H NMR spectrum of receptor **5**.

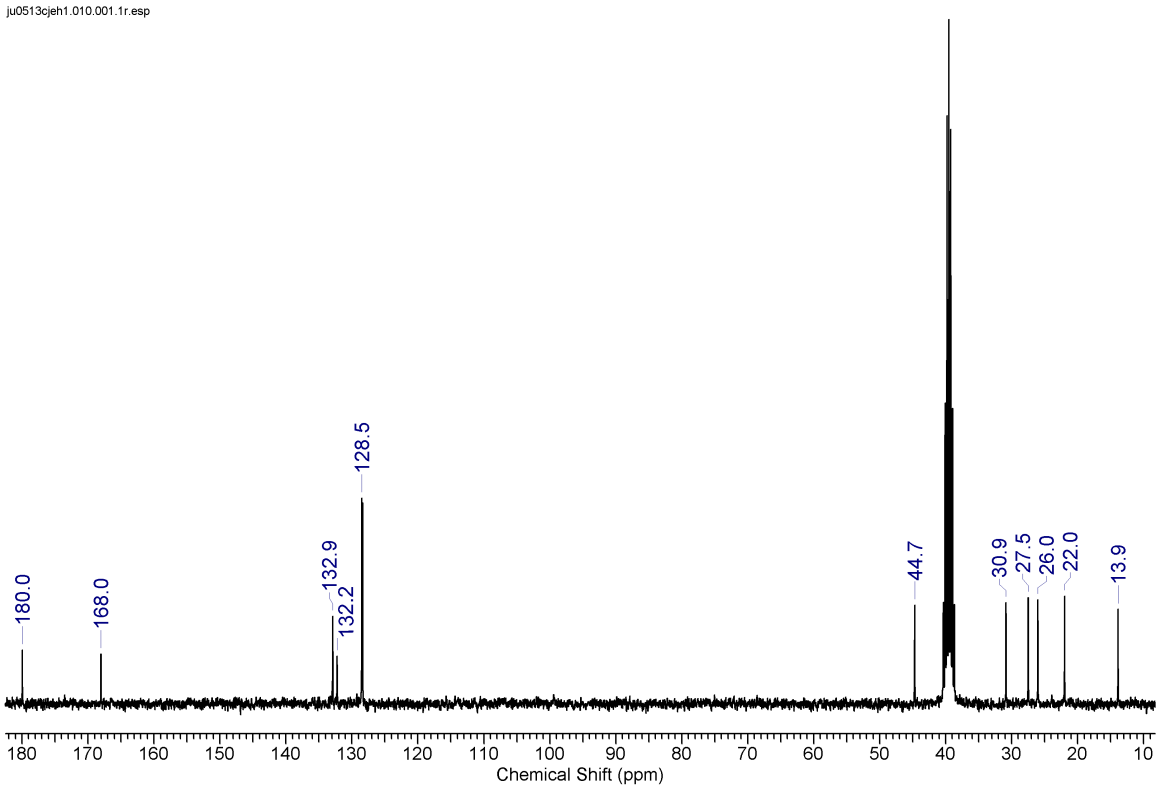

Fig. S2 The ^{13}C NMR spectrum of receptor **5**.

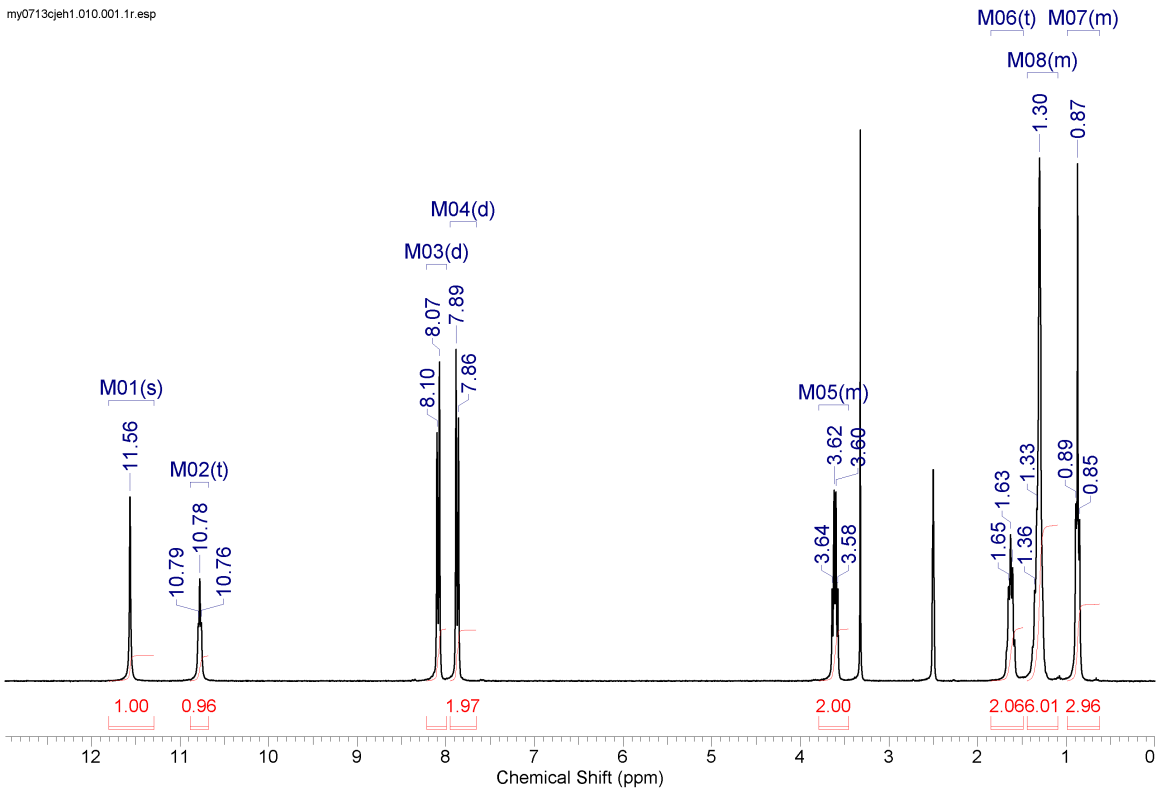

Fig. S3 The ^{1}H NMR spectrum of receptor **6**.

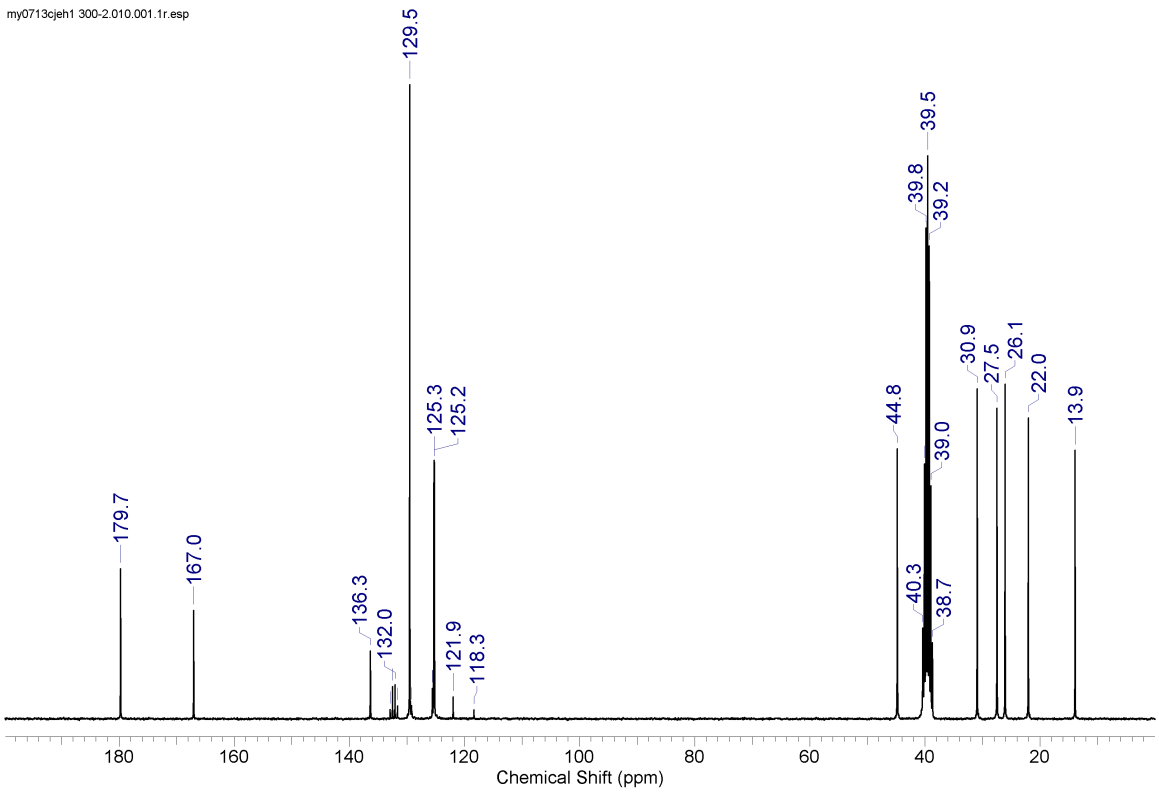

Fig. S4 The ^{13}C NMR spectrum of receptor **6**.

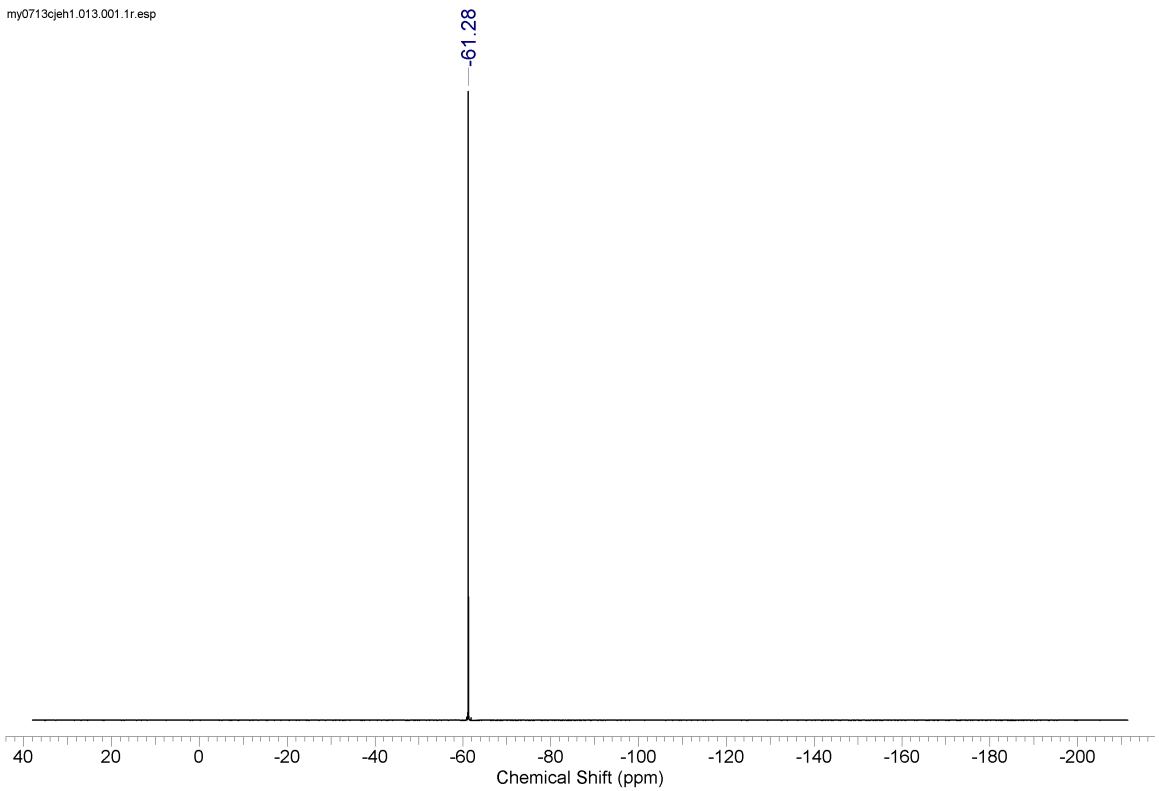

Fig. S5 The ^{19}F NMR spectrum of receptor **6**.

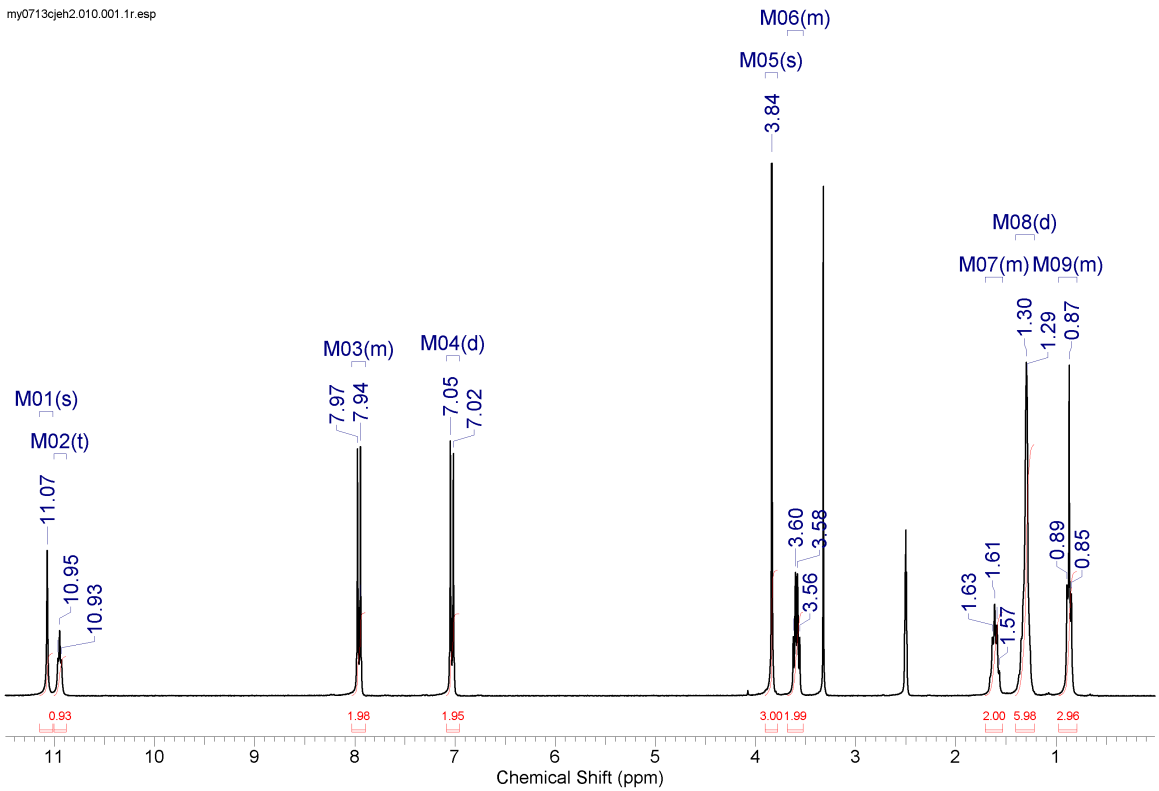

Fig. S6 The ^{1}H NMR spectrum of receptor **7**.

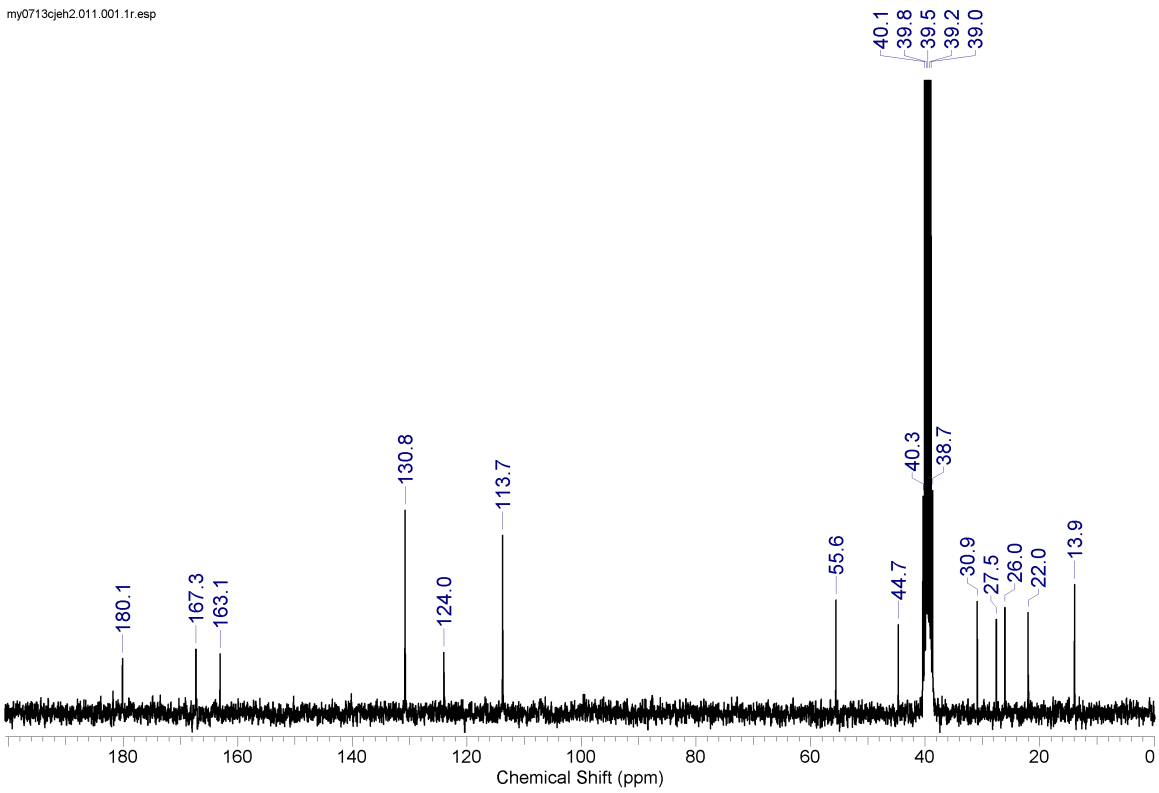

Fig. S7 The ^{13}C NMR spectrum of receptor **7**.

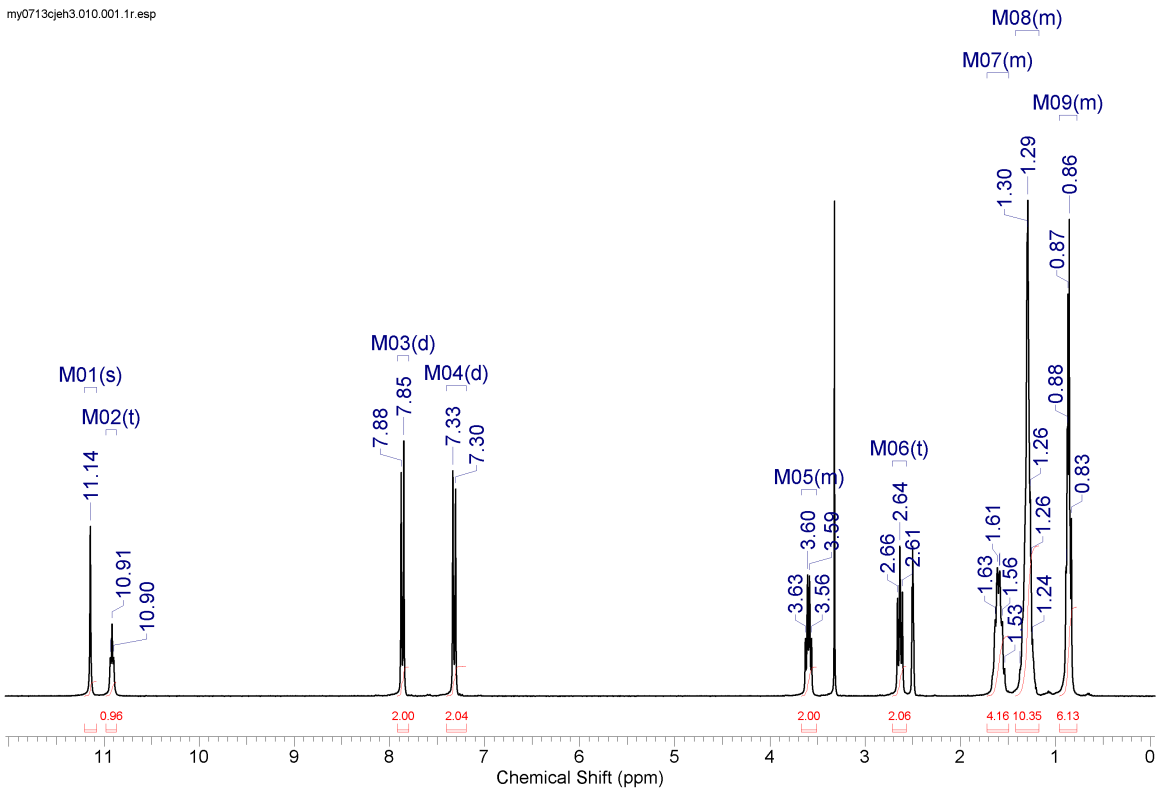

Fig. S8 The ^{1}H NMR spectrum of receptor **8**.

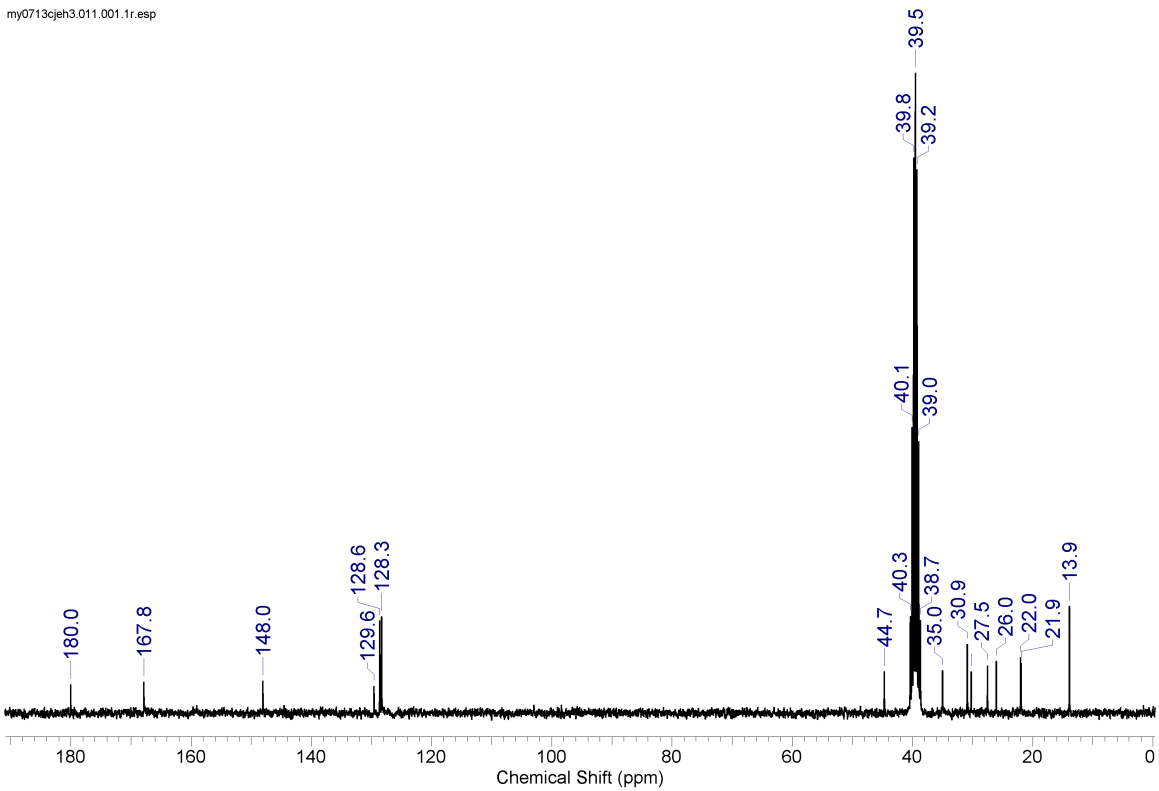

Fig. S9 The ^{13}C NMR spectrum of receptor **8**.

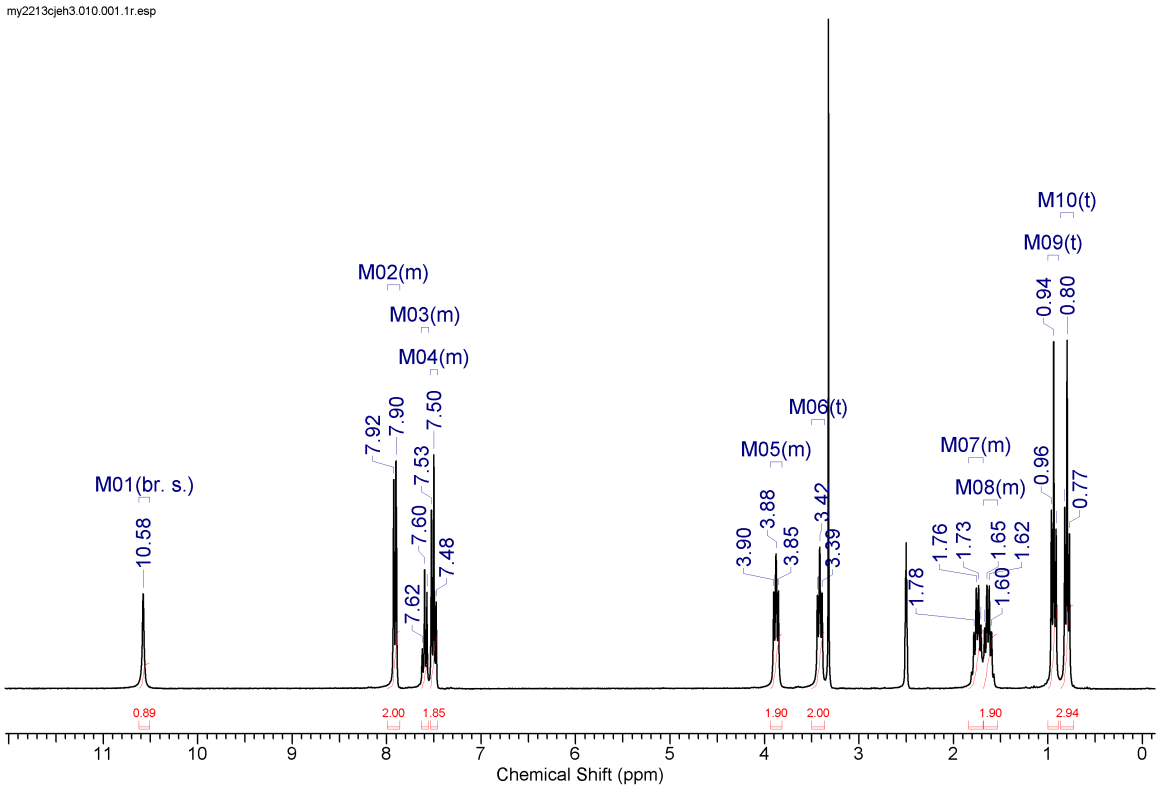

Fig. S10 The ^{1}H NMR spectrum of receptor **9**.

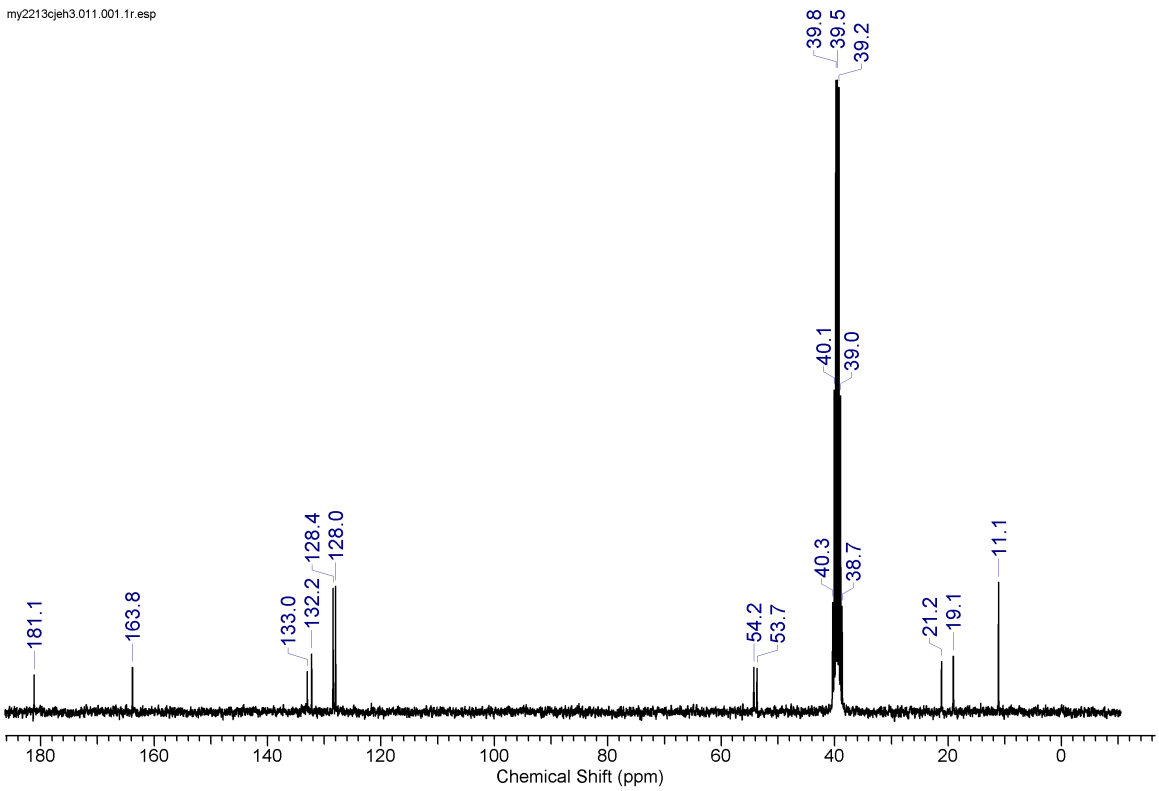

Fig. S11 The ^{13}C NMR spectrum of receptor **9**.

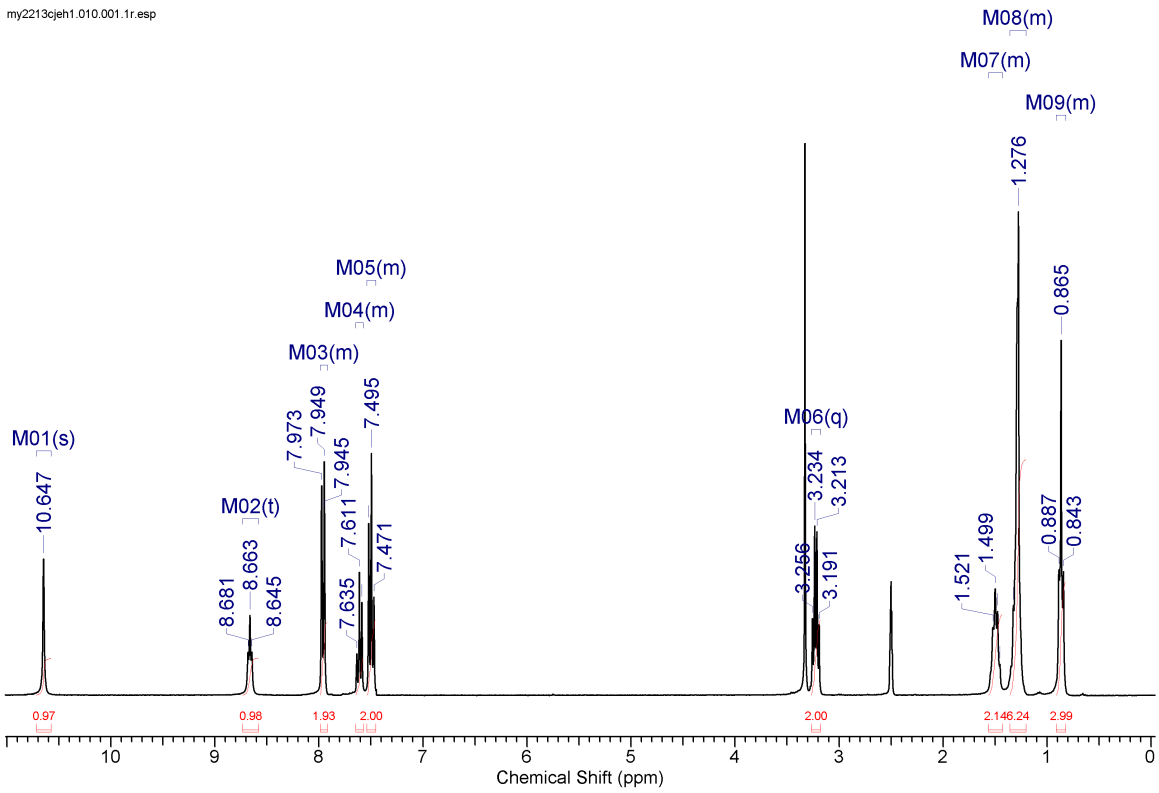

Fig. S12 The ^{1}H NMR spectrum of receptor **10**.

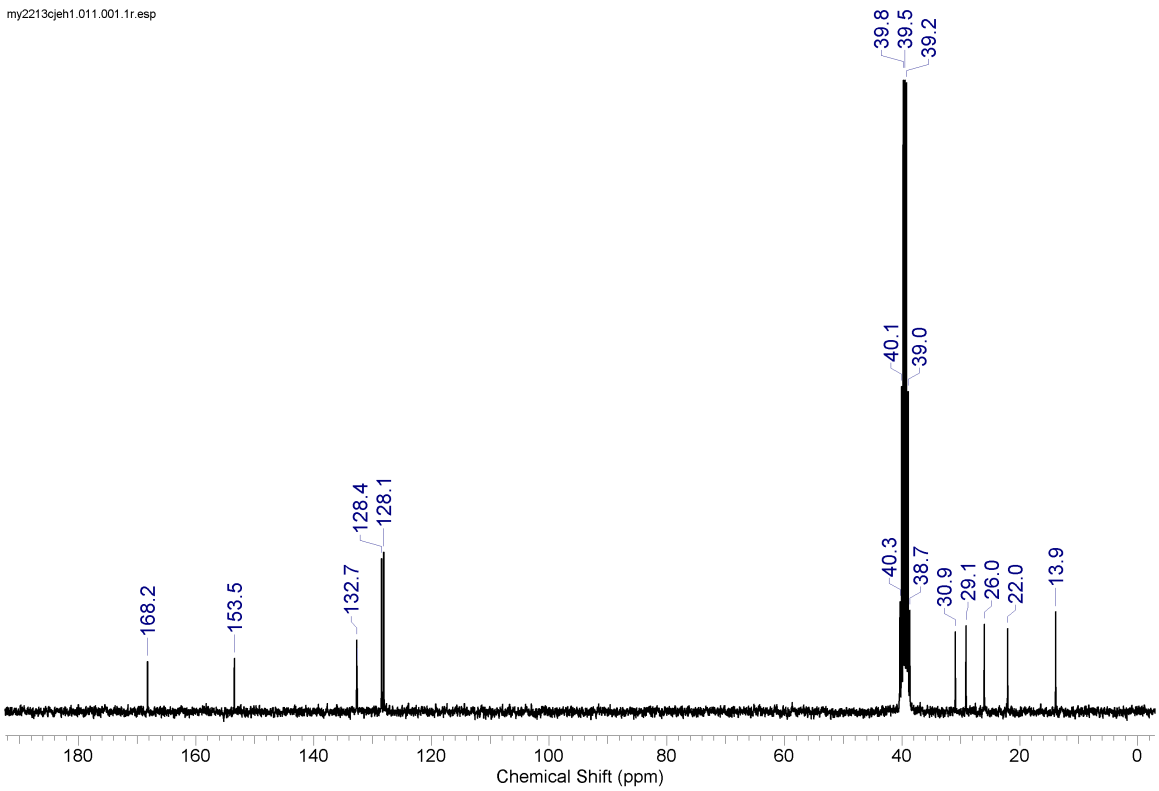

Fig. S13 The ^{13}C NMR spectrum of receptor **10**.

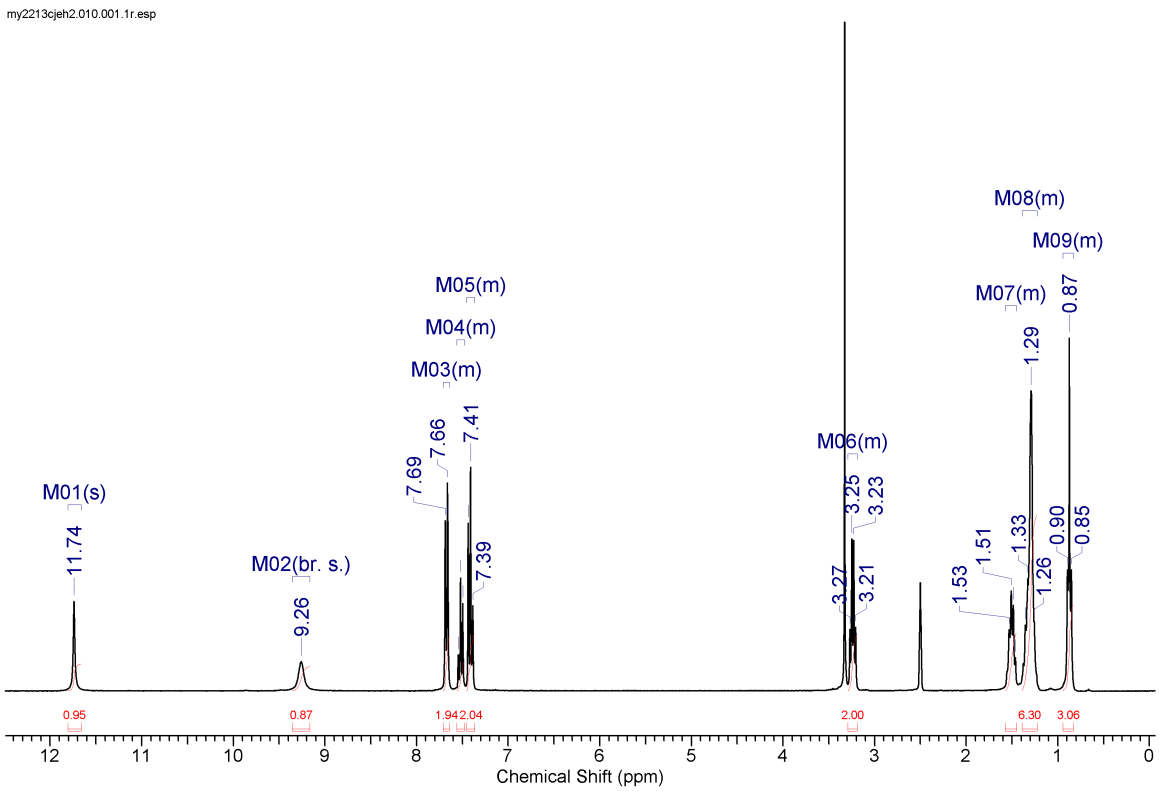

Fig. S14 The ^{1}H NMR spectrum of receptor **11**.

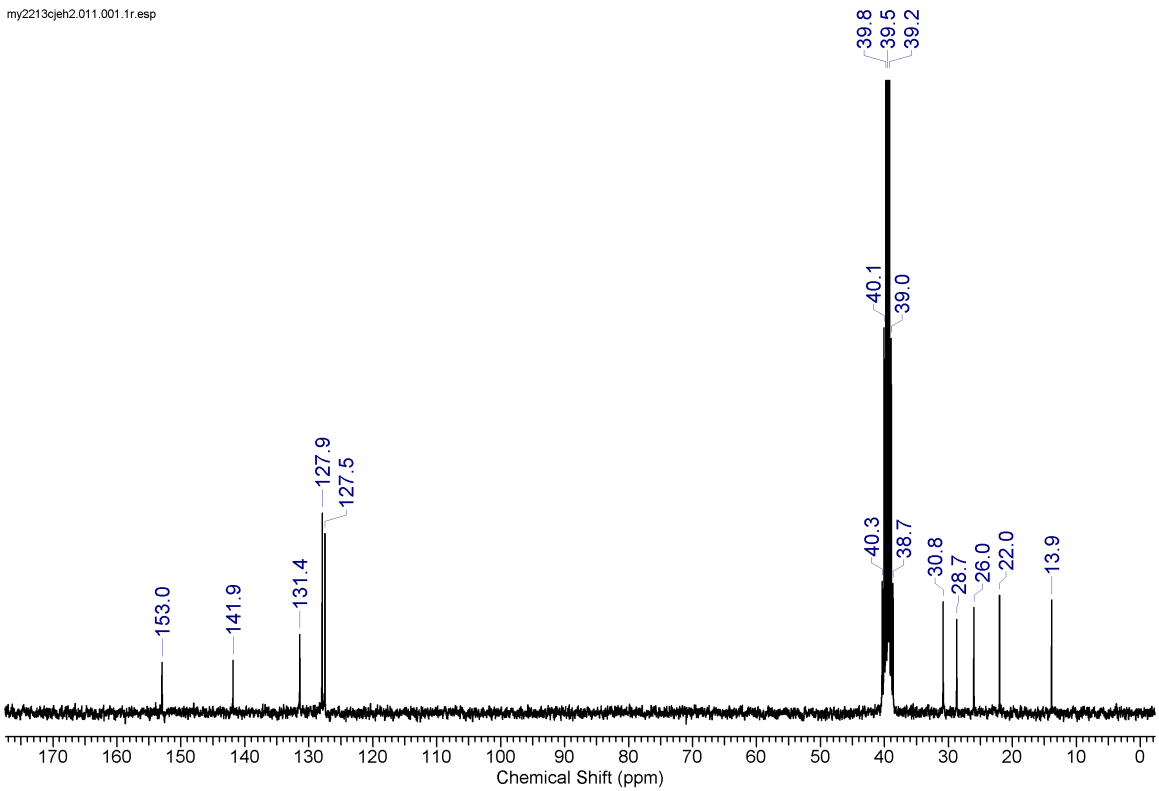

Fig. S15 The ^{13}C NMR spectrum of receptor **11**.

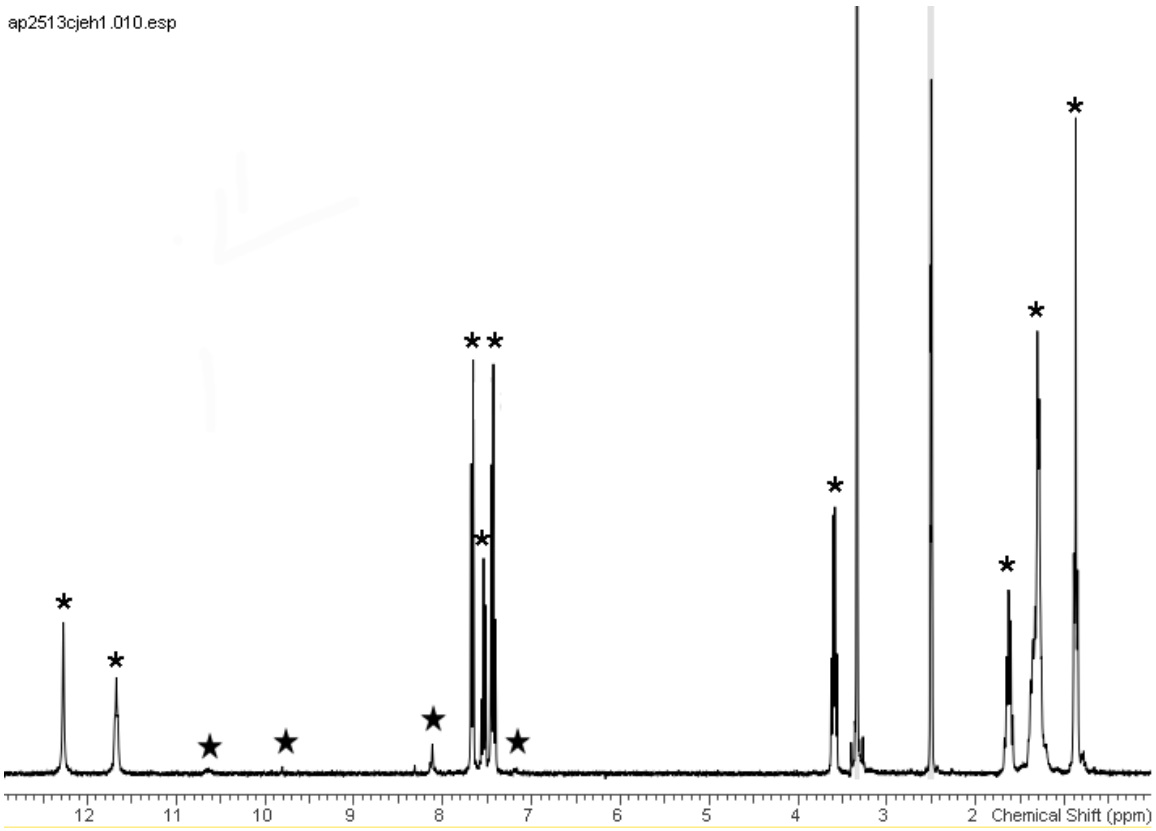

Fig. S16 The ^{1}H NMR spectrum of receptor **12**. Peaks marked * are thought to be associated with the desired receptor, peaks marked ★ are impurities, some of which only appeared during attempted purification.

4 COSY NMR spectra

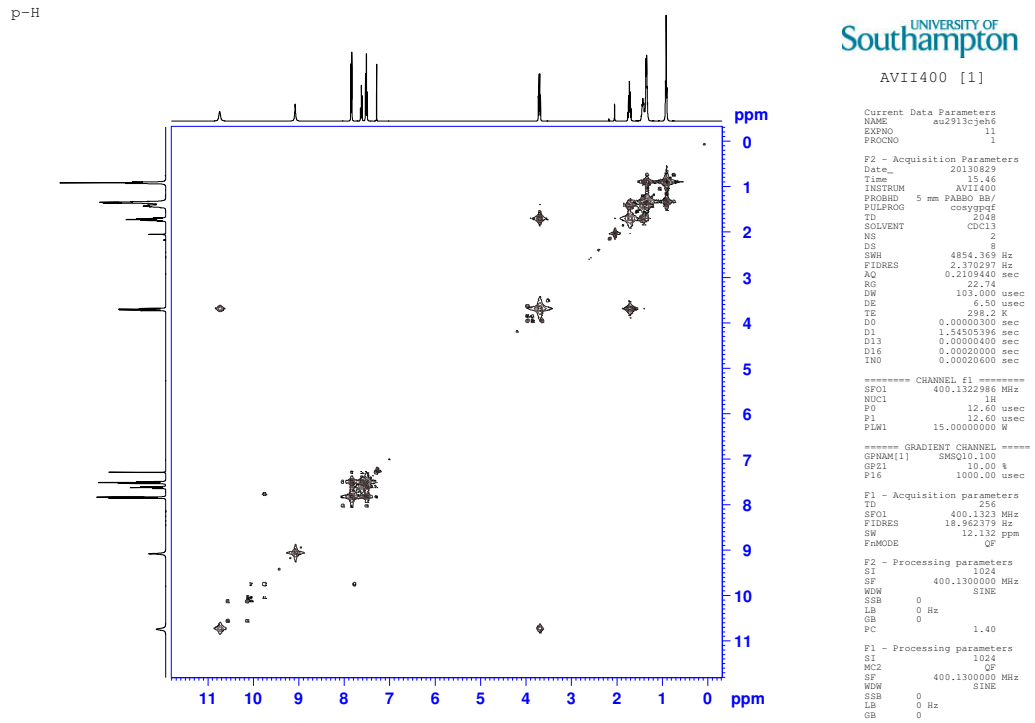

Fig. S17 COSY NMR spectrum of receptor **5** in $CDCl_3$

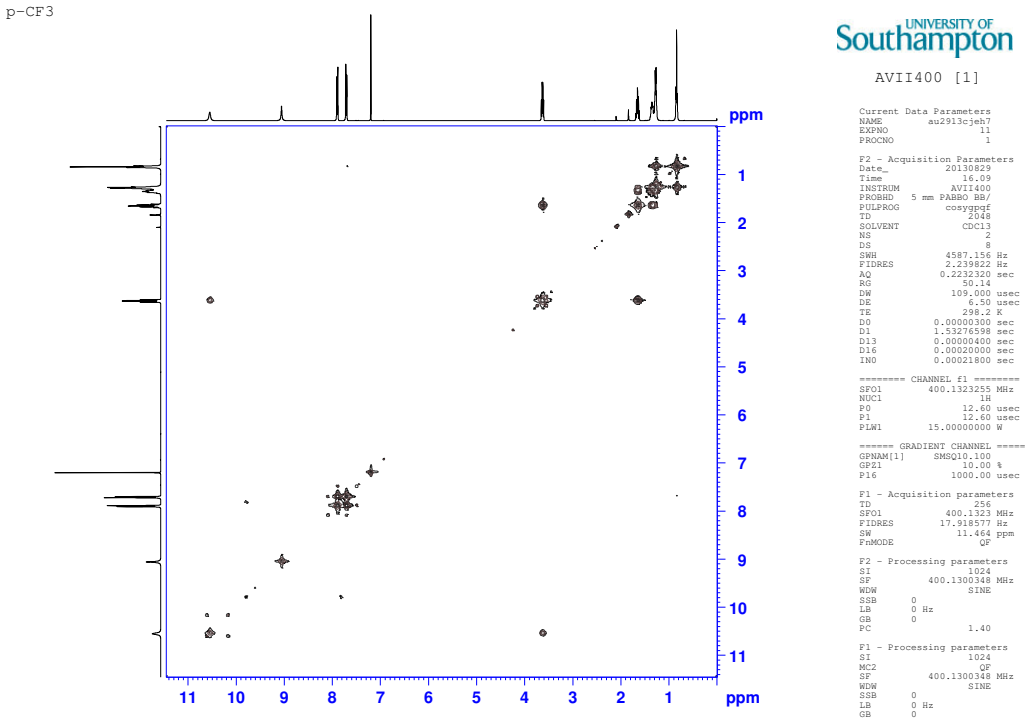

Fig. S18 COSY NMR spectrum of receptor **6** in $CDCl_3$

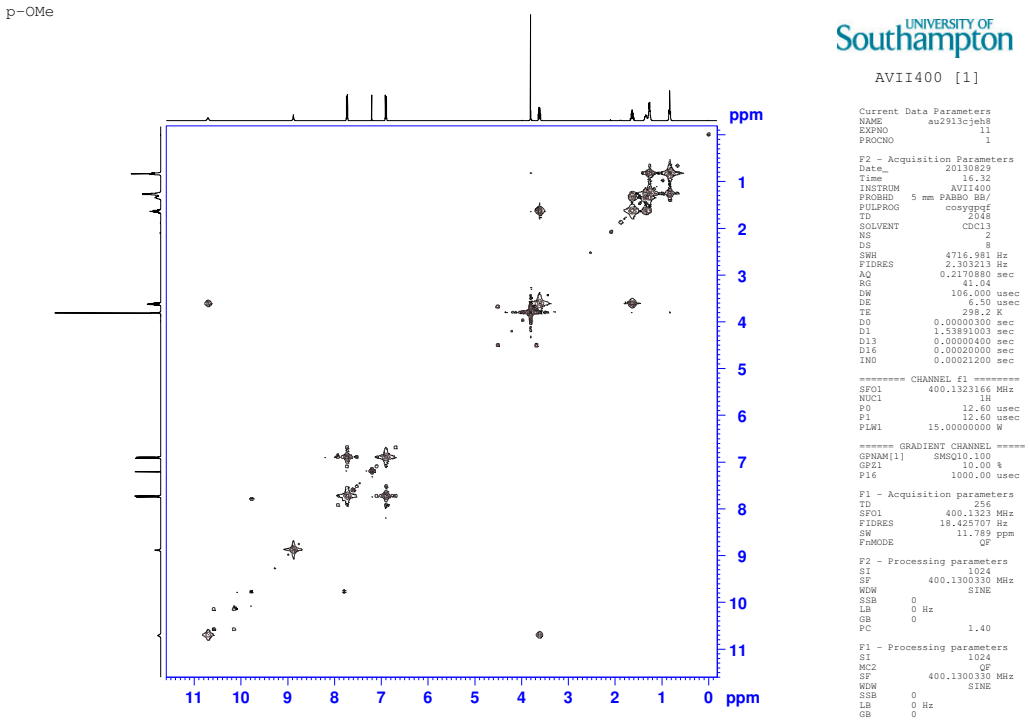

Fig. S19 COSY NMR spectrum of receptor **7** in $CDCl_3$

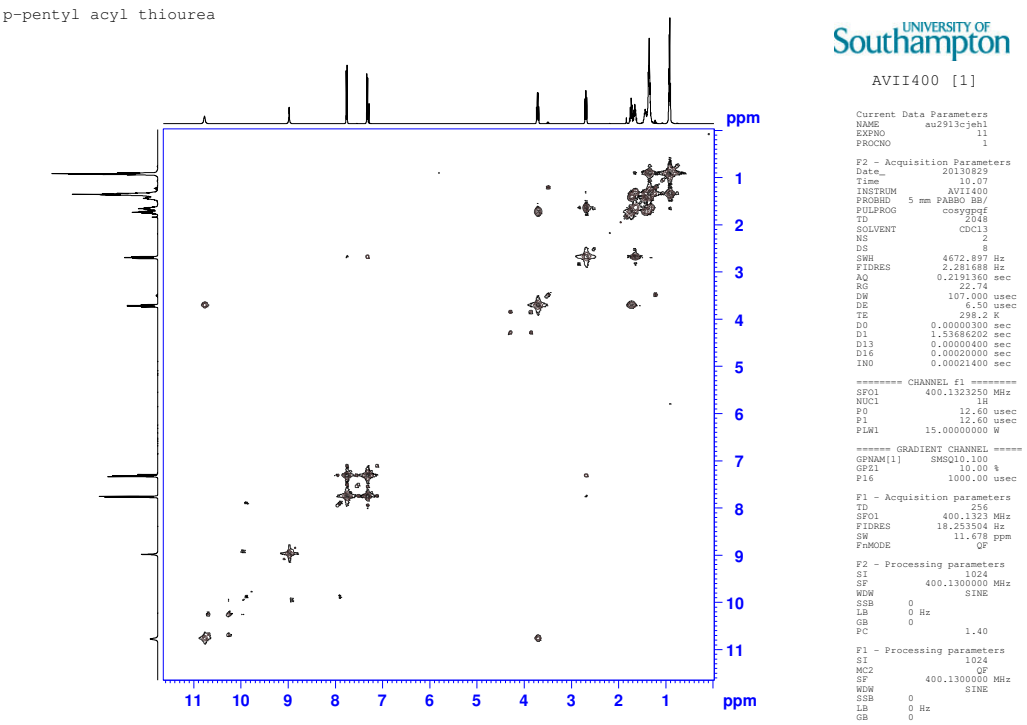

Fig. S20 COSY NMR spectrum of receptor **8** in $CDCl_3$

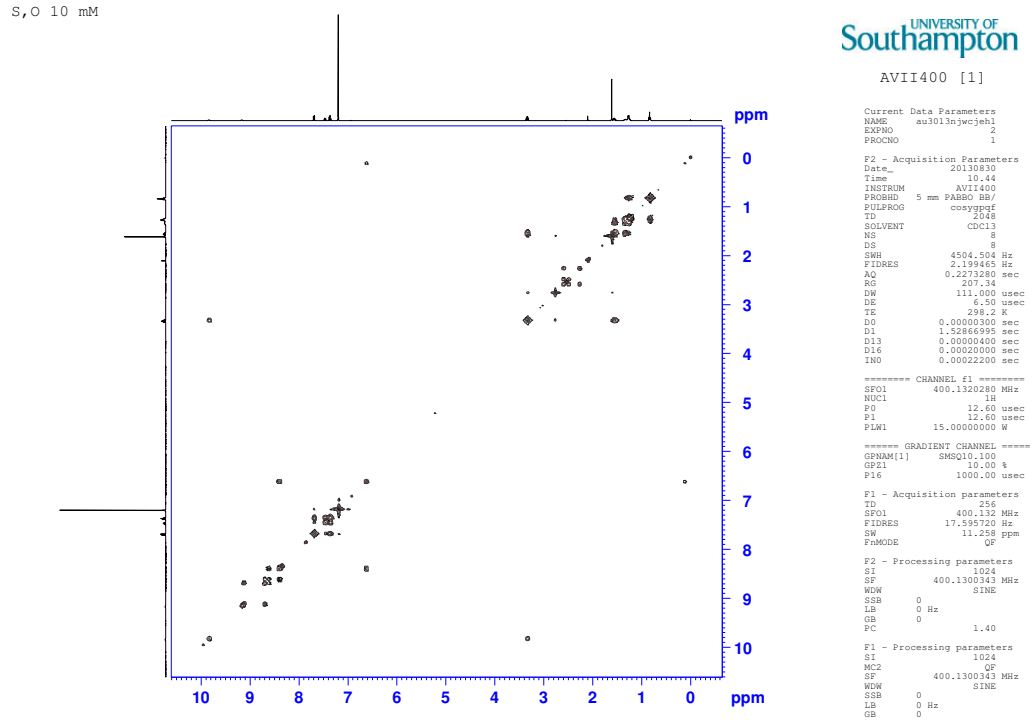

Fig. S21 COSY NMR spectrum of receptor **11** in $CDCl_3$.

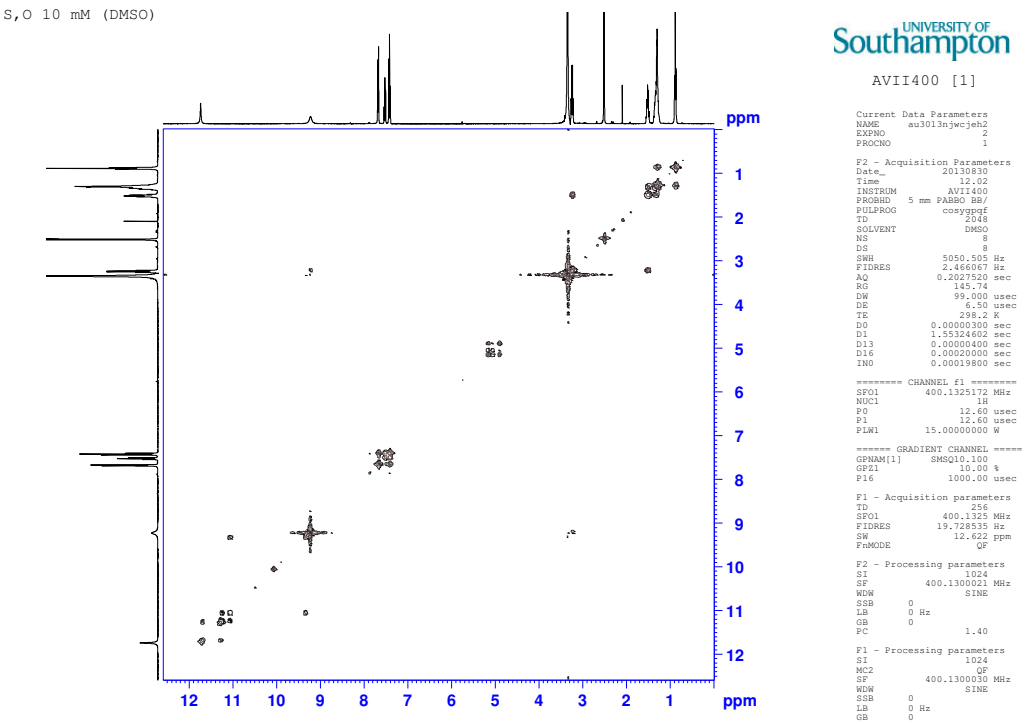

Fig. S22 COSY NMR spectrum of receptor **11** in DMSO-d_6.

5 Single Crystal X-ray Diffraction

Data were collected at the University of Southampton on a *Rigaku AFC12* goniometer equipped with an enhanced sensitivity (HG) *Saturn724+* detector mounted at the window of an *FR-E+ SuperBright* molybdenum rotating anode generator with VHF *Varimax* optics (70 µm focus). Cell determination, data collection, data reduction and cell refinement and absorption correction were performed using CrystalClear-SM Expert 2.0 r7 (Rigaku, 2011). The structures were solved using SHELXS-97 (G. M. Sheldrick, Acta Cryst. (2008) A64 112-122) and refined on *F2* by the full-matrix least-squares technique using the SHELXL-97 program package (G. M. Sheldrick (1997), University of Göttingen, Germany). Graphics are generated using ORTEP-III, MERCURY 3.0 or ViewerLite and Pov-Ray. In all cases the non-hydrogen atoms are refined anisotropically till convergence. Hydrogen atoms were stereochemically fixed at idealized positions and then refined isotropically. Hydrogen bonds are calculated using HTAB command in SHELXL-97. Structures were deposited with the Cambridge Crystallographic Database Centre (CCDC) and given the numbers CCDC 941594-941597.

X-ray data for compound 6, CCDC 941595

Single crystals suitable for X-ray diffraction were obtained by slow evaporation of a solution of compound **6** in DCM. Crystal data for compound **6**: $C_{15}H_{19}F_3N_2OS$, M_r = 332.39 g/mol, crystal size = 0.26 x 0.06 x 0.01 mm³, colourless plate, triclinic, space group *P-1*, a = 9.6713(7) Å, b = 12.2170(9) Å, c = 14.0933(11) Å, α = 95.844(7) º, β = 92.324(7) º, γ = 104.975(7) º, V = 1596.4(2) Å^3, Z = 4, ρ_c = 1.383 g cm^{-3}, μ = 0.236 mm^{-1}, radiation and wavelength = MoK\a (0.71075), T = 100(2) K, θ_{max} = 27.48, reflections collected: 14983, independent reflections: 7217 (R_{int} = 0.0383), 397 parameters, R indices (all data): R_1 = 0.0626, wR_2 = 0.1175, final R indices [$I > 2\sigma I$]: R_1 = 0.0435, wR_2 = 0.1086, *GOOF* = 1.039, largest diff. peak and hole = 0.324 and -0.404 e Å³.

Table S1. Hydrogen bond properties for **6**

Donor--H···Acceptor	D-H (Å)	H···A (Å)	D···A (Å)	D-H···A (°)
N1-H1···S1	0.88	2.61	3.4905(14)	176.4
N4-H4A···O2	0.88	1.92	2.6194(17)	134.8
N2-H2···O1	0.88	1.93	2.6204(17)	134.4

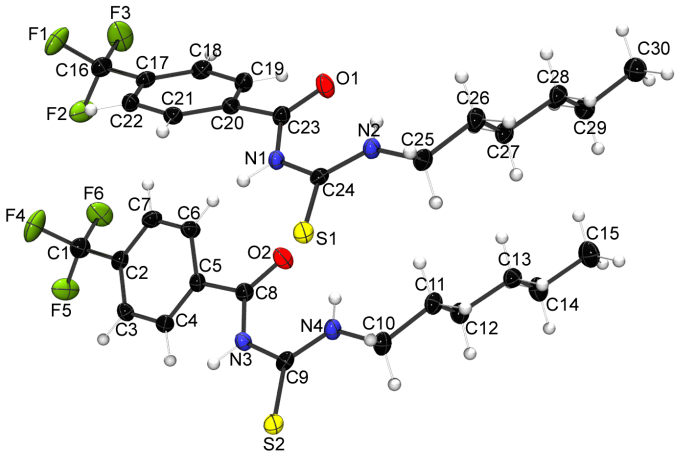

Figure S23. ORTEP diagram of **6** with atom numbering, showing 50% probability factor for the thermal ellipsoids.

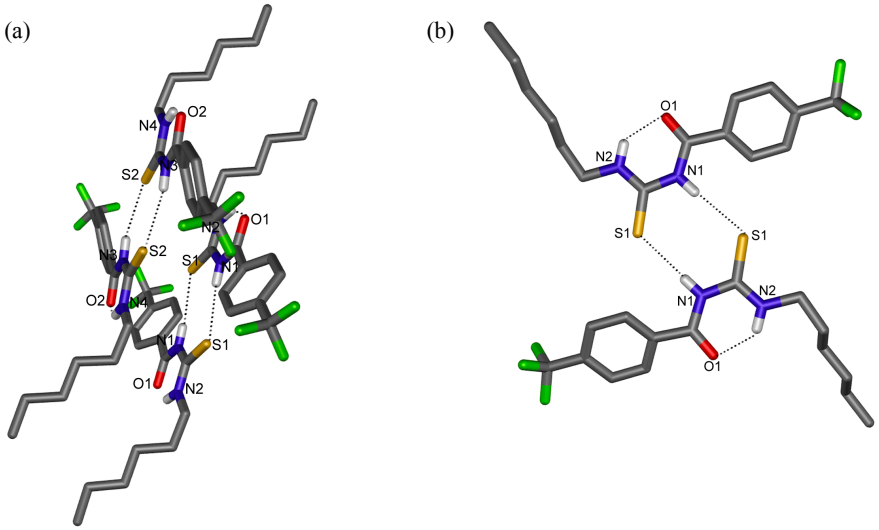

Figure S24. Schematic representation of the intermolecular hydrogen bonds in the crystal of **6** (two different views (a) and (b)). For clarity, only atoms involved in hydrogen bonding are labeled. Hydrogen bonds are represented by dashed lines.

X-ray data for compound 7, CCDC 941596

Single crystals suitable for X-ray diffraction were obtained by slow evaporation of a solution of compound **7** in DCM. Crystal data for compound **7**: $C_{15}H_{22}N_2O_2S$, M_r = 294.41 g/mol, crystal size = 0.06 x 0.04 x 0.01 mm³, colourless chip, monoclinic, space group *P21/c*, a = 18.395(8) Å, b = 8.682(4) Å, c = 9.855(5) Å, α = 90 º, β = 98.783(6) º, γ = 90 º, V = 1555.4(12) Å^3, Z = 4, ρ_c = 1.257 g cm^{-3}, μ = 0.212 mm^{-1}, radiation and wavelength = MoK\a (0.71075), T = 100(2) K, θ_{max} = 25.34, reflections collected: 9085, independent reflections: 2842 (R_{int} = 0.1258), 196 parameters, R indices (all data): R_1 = 0.0810, wR_2 = 0.1388, final R indices [$I > 2\sigma I$]: R_1 = 0.0614, wR_2 = 0.1513, *GOOF* = 1.003, largest diff. peak and hole = 0.340 and -0.271 e Å³. The hexyl chain was found to be disorder and was modeled with 2 separate orientations.

Table S2. Hydrogen bond properties for **7**

Donor--H···Acceptor	D-H (Å)	H···A (Å)	D···A (Å)	D-H···A (°)
N1-H1···O1	0.88	2.28	3.116(3)	159.4
N2-H2A···O1	0.88	2.00	2.678(3)	133.4
N2-H2A···S1	0.88	2.77	3.431(3)	133.1

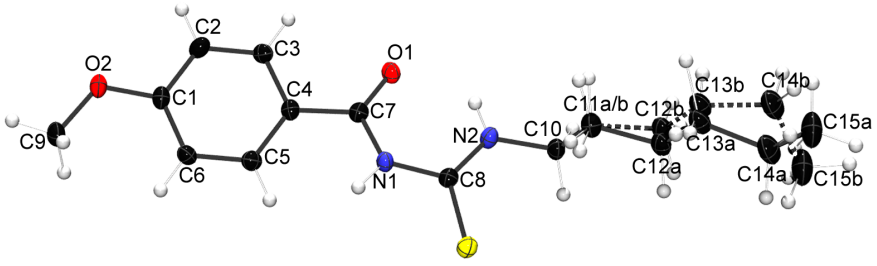

Figure S25. ORTEP diagram of **7** with atom numbering, showing 50% probability factor for the thermal ellipsoids.

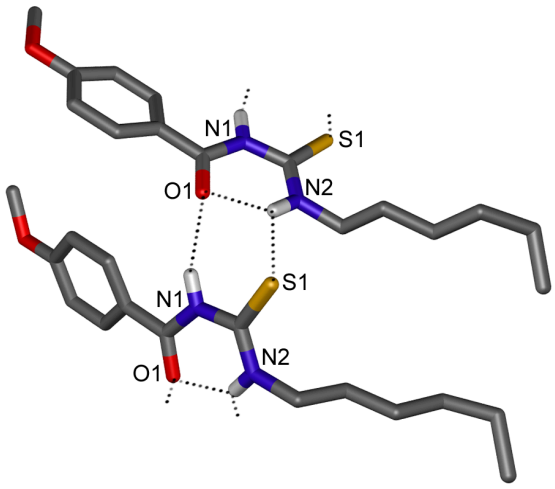

Figure S26. Schematic representation of the intermolecular hydrogen bonds in the crystal of **7**. For clarity, only atoms involved in hydrogen bonding are labeled. Hydrogen bonds are represented by dashed lines.

X-ray data for compound 10, CCDC 941597

Single crystals suitable for X-ray diffraction were obtained by slow evaporation of a solution of compound **10** in DCM. Crystal data for compound **10**: $C_{14}H_{20}N_2O_2$, M_r = 248.32 g/mol, crystal size = 0.20 x 0.06 x 0.02 mm³, colourless lath, monoclinic, space group *P21/c*, a = 5.166(3) Å, b = 34.07(2) Å, c = 7.566(5) Å, α = 90 º, β = 101.193(10) º, γ = 90 º, V = 1306.3(14)) Å^3, Z = 4, ρ_c = 1.263 g cm^{-3}, μ = 0.085 mm^{-1}, radiation and wavelength = MoK\a (0.71075), T = 100(2) K, θ_{max} = 25.02, reflections collected: 4606, independent reflections: 2078 (R_{int} = 0.0389), 164 parameters, R indices (all data): R_1 = 0.0708, wR_2 = 0.1083, final R indices [$I > 2\sigma I$]: R_1 = 0.0510, wR_2 = 0.0988, *GOOF* = 1.038, largest diff. peak and hole = 0.193 and -0.194 e Å³.

Table S3. Hydrogen bond properties for **10**

Donor--H···Acceptor	D-H (Å)	H···A (Å)	D···A (Å)	D-H···A (°)
N1-H1···O1	0.88	2.21	3.029(3)	153.8
N2-H2···O1	0.88	2.08	2.730(2)	129.7
N2-H2···O2	0.88	2.33	2.941(3)	126.4

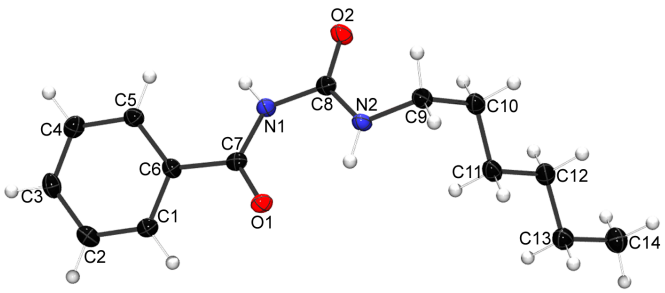

Figure S27. ORTEP diagram of **10** with atom numbering, showing 50 % probability factor for the thermal ellipsoids.

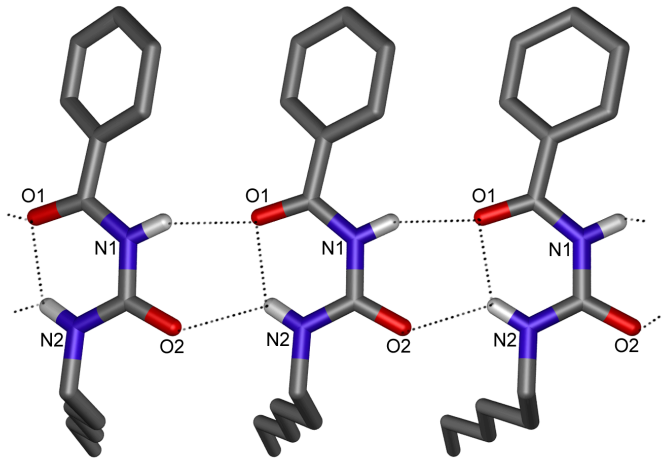

Figure S28. Schematic representation of the intermolecular hydrogen bonds in the crystal of **10**. For clarity, only atoms involved in hydrogen bonding are labeled and disorder is omitted. Hydrogen bonds are represented by dashed lines.

X-ray data for compound 11, CCDC 941594

Single crystals suitable for X-ray diffraction were obtained by slow evaporation of a solution of compound **11** in 3:1 DCM:hexane. Crystal data for compound **11**: $C_{14}H_{20}N_2OS$, M_r = 264.38 g/mol, crystal size = 0.55 x 0.04 x 0.01 mm³, yellow needle, monoclinic, space group *P21/c*, a = 3.9805(12) Å, b = 21.132(7) Å, c = 16.710(5) Å, α = 90 º, β = 96.391(4) º, γ = 90 º, V = 1396.8(8) Å^3, Z = 4, ρ_c = 1.257 g cm^{-3}, μ = 0.223 mm^{-1}, radiation and wavelength = MoK\a (0.71075), T = 100(2) K, θ_{max} = 27.52, reflections collected: 6301, independent reflections: 3169 (R_{int} = 0.0185), 163 parameters, R indices (all data): R_1 = 0.0459, wR_2 = 0.0871, final R indices [$I > 2\sigma I$]: R_1 = 0.0393, wR_2 = 0.0834, *GOOF* = 1.072, largest diff. peak and hole = 0.354 and -0.232 e Å³.

Table S4. Hydrogen bond properties for **11**

Donor--	D-H (Å)	H···A (Å)	D···A (Å)	D-H···A (°)
N2-H2···S1	0.88	2.28	3.0046(15)	140.2
N1-H1···O1	0.88	2.01	2.8672(15)	166.0

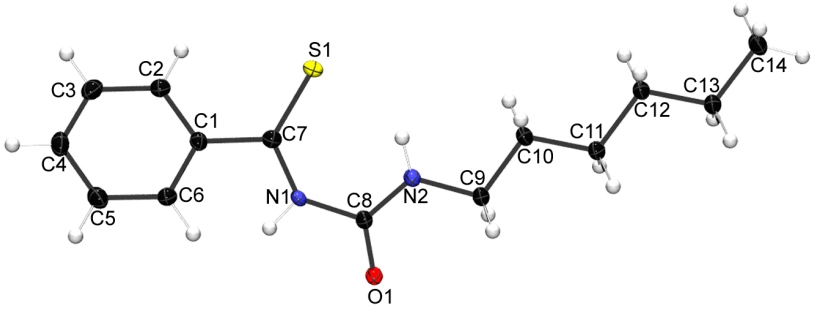

Figure S29. ORTEP diagram of **11** with atom numbering, showing 50 % probability factor for the thermal ellipsoids.

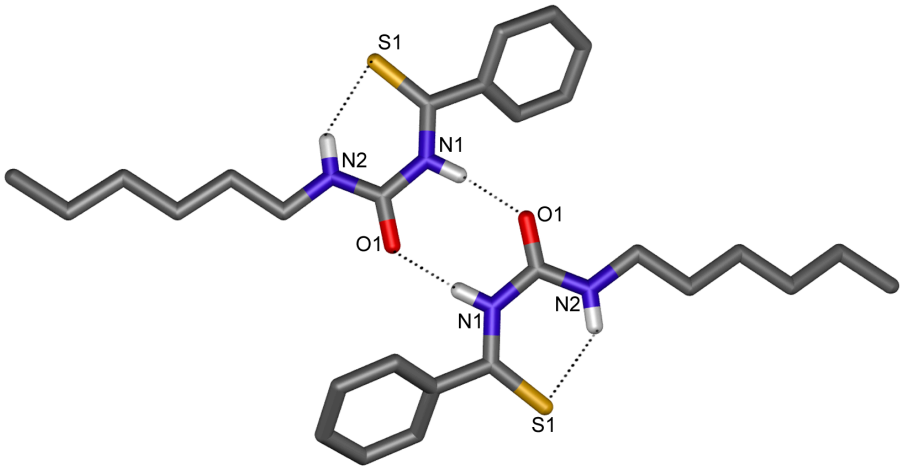

Figure S30. Schematic representation of the intermolecular hydrogen bonds in the crystal of **11**. For clarity, only atoms involved in hydrogen bonding are labeled and disorder is omitted. Hydrogen bonds are represented by dashed lines.

6 D_2O shake experiments (5 mL of 0.01 M receptor in DMSO-d_6)

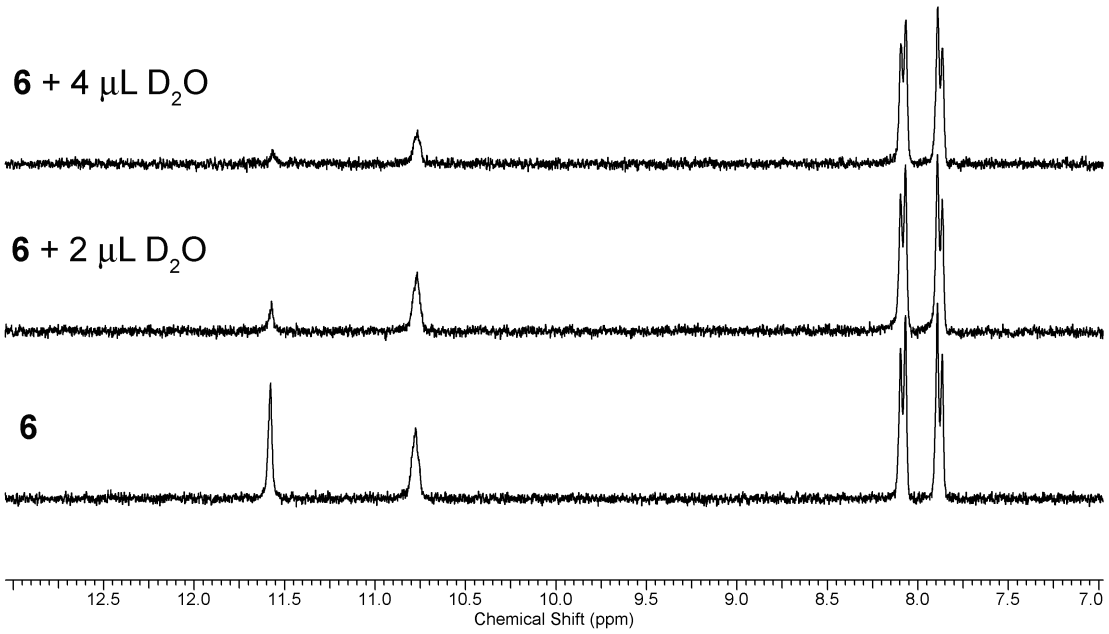

Fig. S31 Changes to the aromatic region of the ^{1}H NMR spectrum of receptor **6** in DMSO-d_6 (0.01 M) upon the addition of D_2O (absolute intensity).

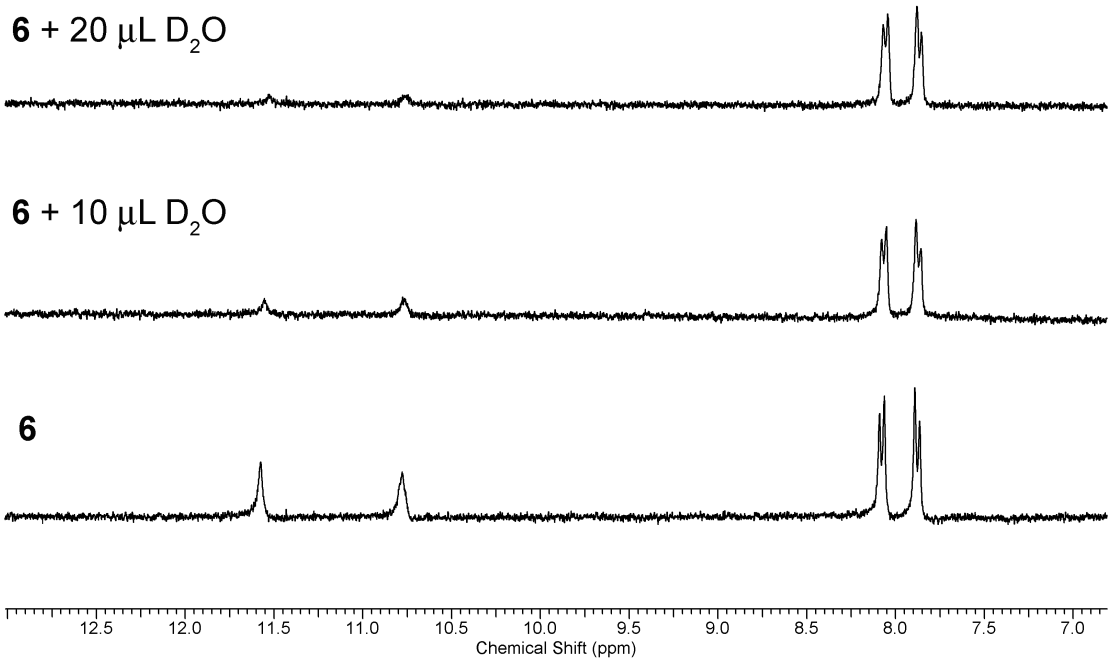

Fig. S32 Changes to the aromatic region of the ^{1}H NMR spectrum of receptor **6** in DMSO-d_6/ 1 % H_2O (0.01 M) upon the addition of D_2O (absolute intensity).

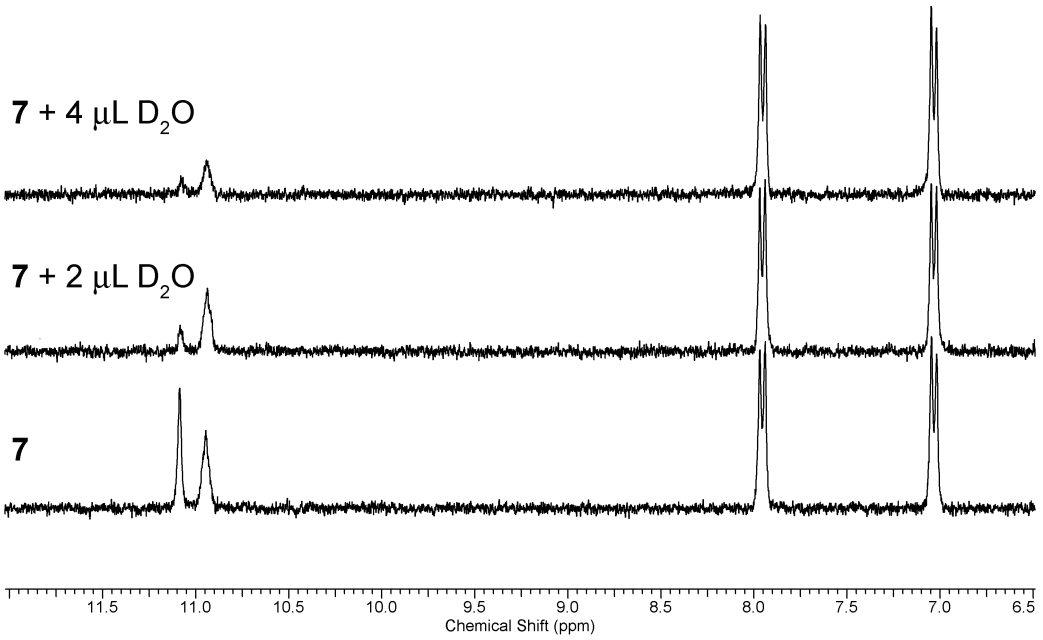

Fig. S33 Changes to the aromatic region of the ^{1}H NMR spectrum of receptor **7** in DMSO-d_6 (0.01 M) upon the addition of D_2O (absolute intensity).

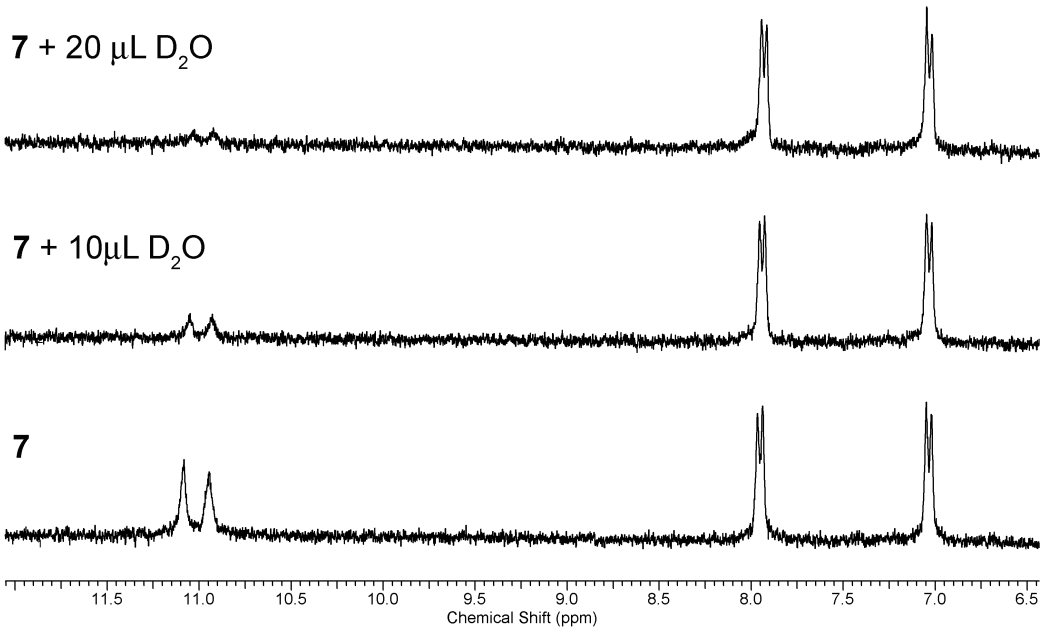

Fig. S34 Changes to the aromatic region of the ^{1}H NMR spectrum of receptor **7** in DMSO-d_6/ 1 % H_2O (0.01 M) upon the addition of D_2O (absolute intensity).

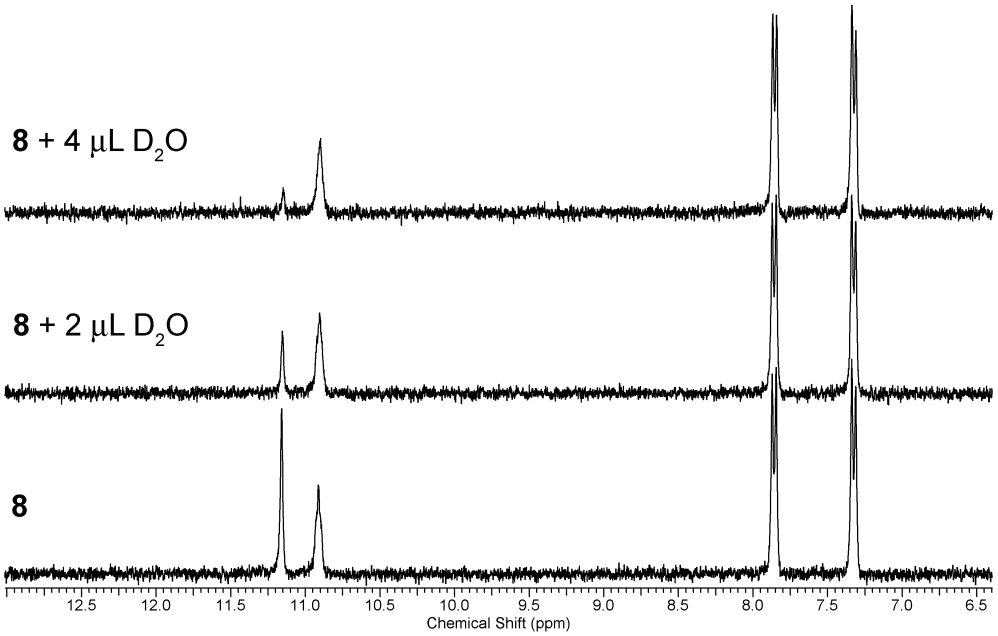

Fig. S35 Changes to the aromatic region of the ^{1}H NMR spectrum of receptor **8** in DMSO-d_6 (0.01 M) upon the addition of D_2O (absolute intensity).

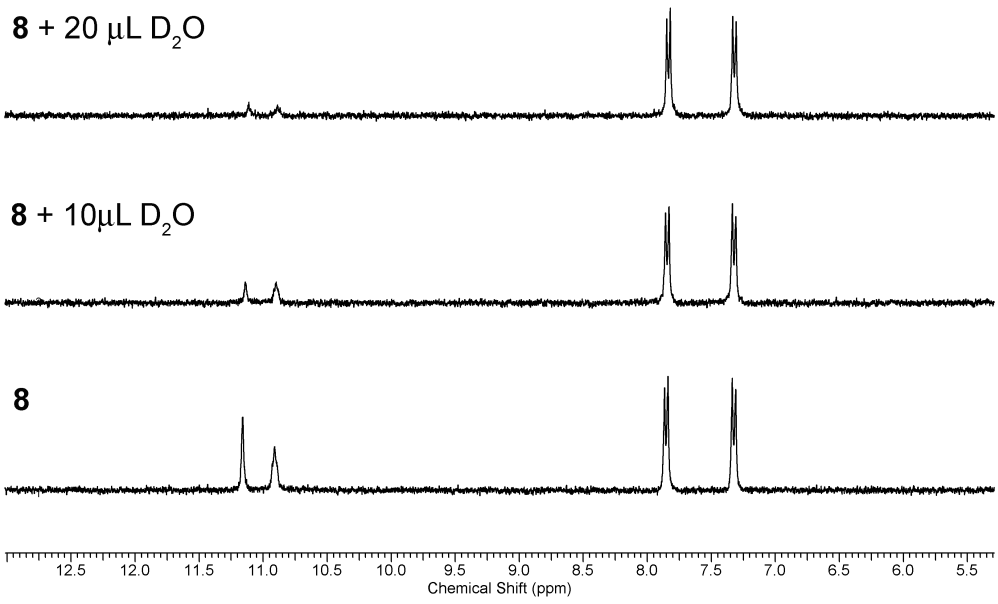

Fig. S36 Changes to the aromatic region of the ^{1}H NMR spectrum of receptor **8** in DMSO-d_6/ 1 % H_2O (0.01 M) upon the addition of D_2O (absolute intensity).

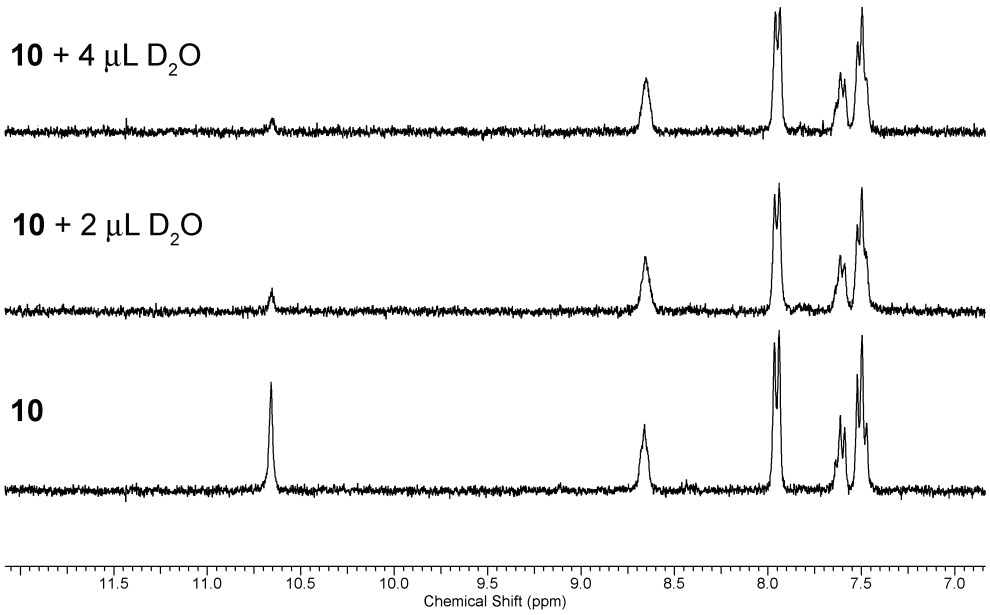

Fig. S37 Changes to the aromatic region of the ^{1}H NMR spectrum of receptor **10** in DMSO-d_6 (0.01 M) upon the addition of D_2O (absolute intensity).

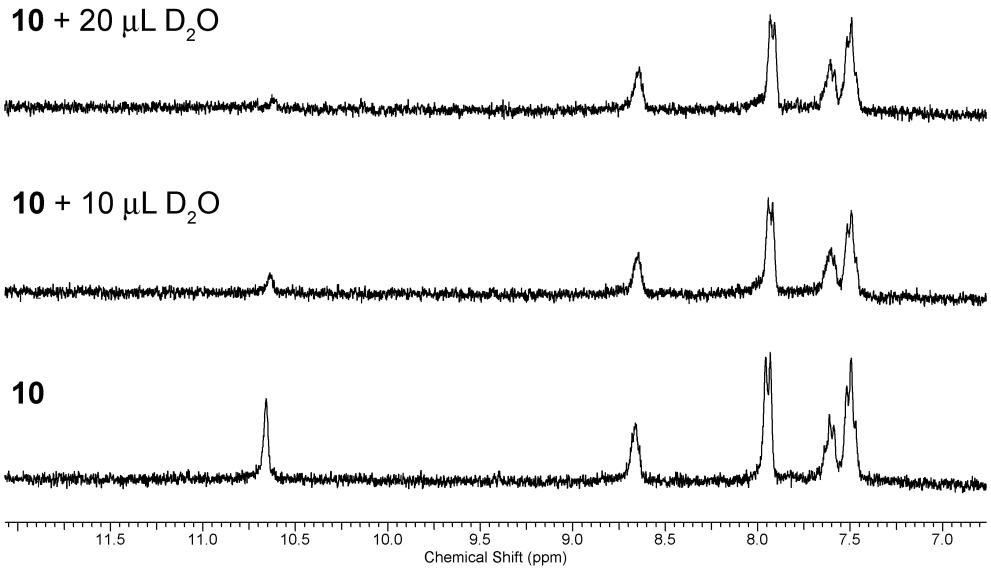

Fig. S38 Changes to the aromatic region of the ^{1}H NMR spectrum of receptor **13** in DMSO-d_6/ 1 % H_2O (0.01 M) upon the addition of D_2O (absolute intensity).

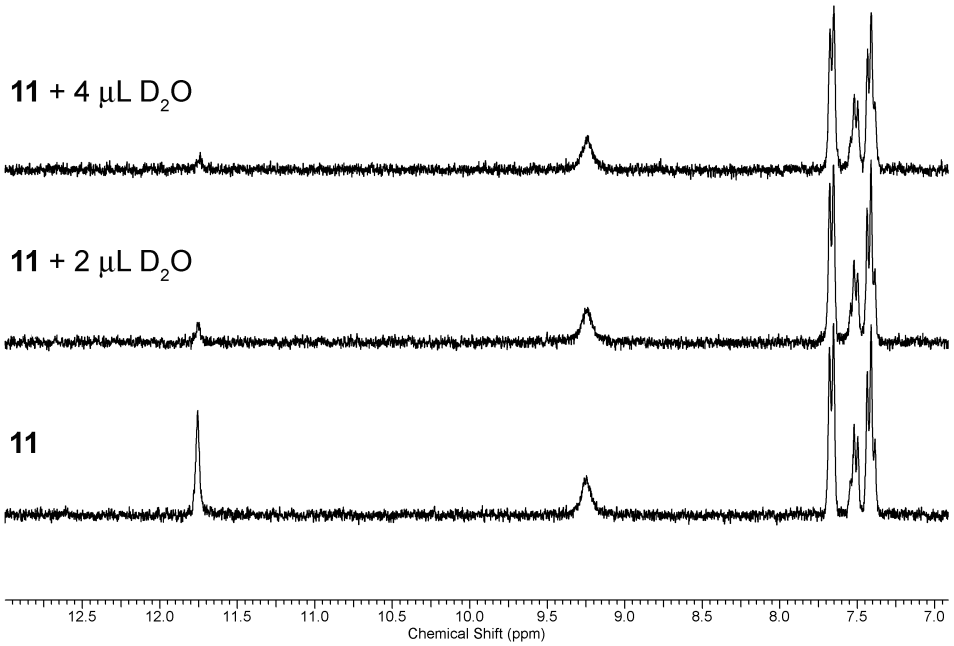

Fig. S39 Changes to the aromatic region of the ^{1}H NMR spectrum of receptor **11** in DMSO-d_6 (0.01 M) upon the addition of D_2O (absolute intensity).

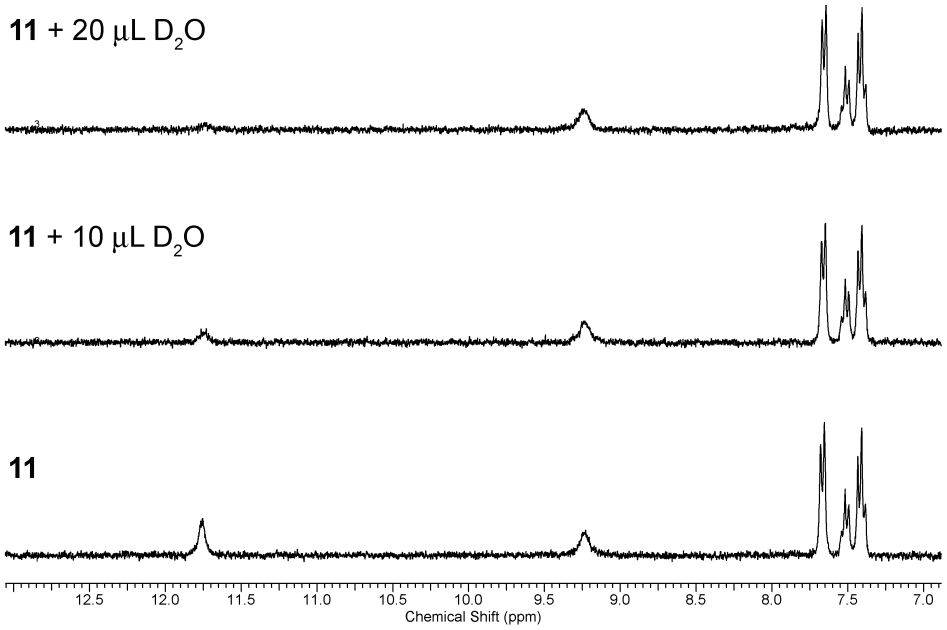

Fig. S40 Changes to the aromatic region of the ^{1}H NMR spectrum of receptor **11** in DMSO-d_6/ 1 % H_2O (0.01 M) upon the addition of D_2O (absolute intensity).

7 Anion transport experiments

7.1 Preparation of vesicles

A lipid film of 1-palmitoyl-2-oleoyl-sn-glycero-3-phosphocholine (POPC) and cholesterol (0% or 30%) was formed from a chloroform solution under reduced pressure and dried under vacuum for at least 4 hours. The lipid film was rehydrated by vortexing with a metal chloride (MCl) salt solution (489 mM MCl, 5 mM phosphate buffer at pH 7.2). The lipid suspension was then subjected to seven freeze-thaw cycles and allowed to age for 30 min at room temperature before extruding 25 times through a 200 nm polycarbonate membrane. The resulting unilamellar vesicles were dialyzed against the external medium to remove unencapsulated MCl salts.

7.2 Cl^-/NO_3^- antiport assays

Unilamellar POPC vesicles containing NaCl, prepared as described above, were suspended in 489 mM $NaNO_3$ buffered to pH 7.2 with sodium phosphate salts. The lipid concentration per sample was 1 mM. A DMSO solution of the carrier molecule (10 mM) was added to start the experiment and the chloride efflux was monitored using a chloride selective electrode. At 5 min, the vesicles were lysed with 50 µl of polyoxyethylene(8)lauryl ether (0.232 mM in 7:1 water:DMSO *v/v*) and a total chloride reading was taken at 7 min.

7.3 Cl^-/HCO_3^- antiport assays

Unilamellar POPC vesicles containing 489 mM NaCl solution buffered to pH 7.2 with 20 mM sodium phosphate salts, prepared as described above, were suspended in the external medium consisting of a 162 mM Na_2SO_4 solution buffered to pH 7.2 with sodium phosphate salts (20 mM buffer). The lipid concentration per sample was 1 mM. A DMSO solution of the carrier molecule (10 mM) was added to start the experiment and chloride efflux was monitored using a chloride sensitive electrode. At 2 min, a $NaHCO_3$ solution (1.2 M in 162 mM Na_2SO_4 buffered to pH 7.2 with 20 mM sodium phosphate salts) was added so that the outer solution contained 40 mM $NaHCO_3$. At 7 min, the vesicles were lysed with 50 µl of polyoxyethylene(8)lauryl ether (0.232 mM in 7:1 water:DMSO *v/v*) and a total chloride reading was taken at 9 min.

7.4 Hill plots

During the Hill plots the chloride/nitrate transport assays were performed as described above (see section 6.1) for various concentrations of carrier. The chloride efflux (%) 270 s after the addition of carrier was plotted as a function of the carrier concentration. Data points were fitted to the Hill equation using Origin 8.1:

$$y = V_{max}\frac{x^n}{k^n + x^n}$$

where y is the chloride efflux at 270 s (%) and x is the carrier concentration (mol% carrier to lipid). Vmax, k and *n* are the parameters to be fitted. V_{max} is the maximum efflux possible (this was fixed to 100%, as this is physically the maximum chloride efflux possible), *n* is the Hill coefficient and k is the carrier concentration needed to reach $V_{max}/2$ (when V_{max} is fixed to 100%, k equals EC_{50}). From the Hill plot it is therefore possible to directly obtain $EC_{50,270s}$ values, defined as the carrier concentration (molar % carrier to lipid) needed to obtain 50 % chloride efflux after 270 s. To ensure repeatability and precise data, each Cl^-/NO_3^- Hill plot was repeated a minimum of 3 times and was conducted each time with a newly prepared set of vesicles.

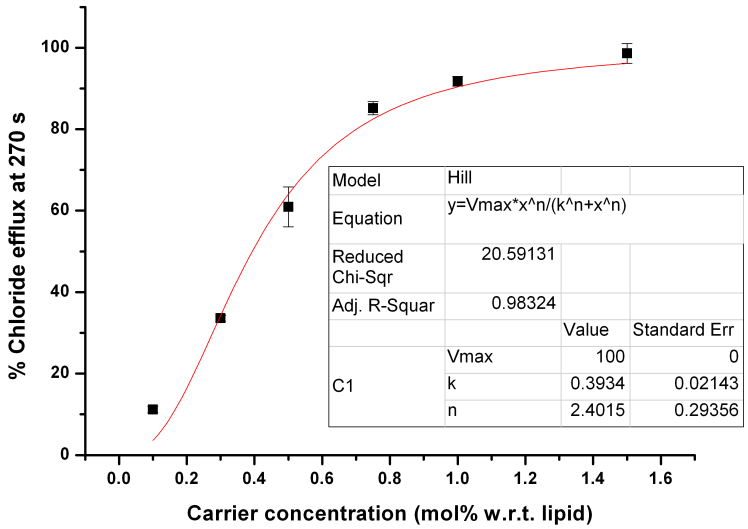

Fig. S41 Hill plot (repeat 1) for Cl^-/NO_3^- antiport by receptor **5**. $EC_{50,\,270\,s}$ = 0.39 mol%, *n* = 2.4.

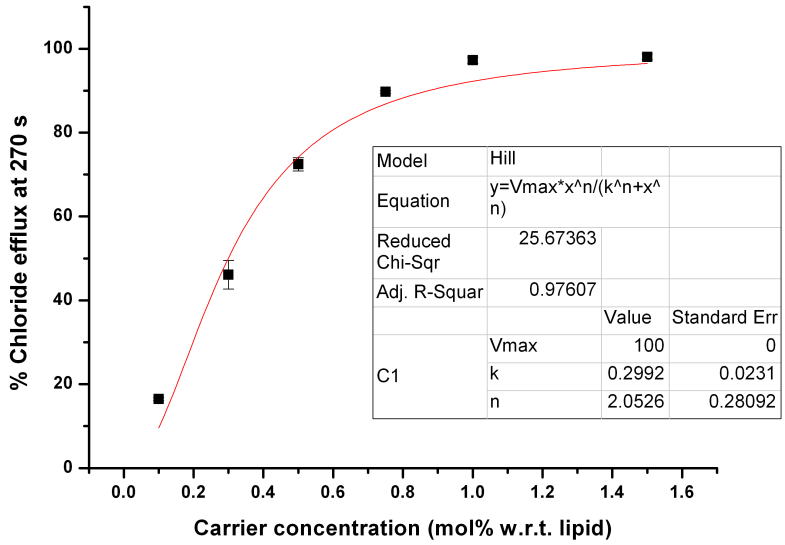

Fig. S42 Hill plot (repeat 2) for Cl^-/NO_3^- antiport by receptor **5**. $EC_{50,\,270\,s}$ = 0.30 mol%, *n* = 2.1.

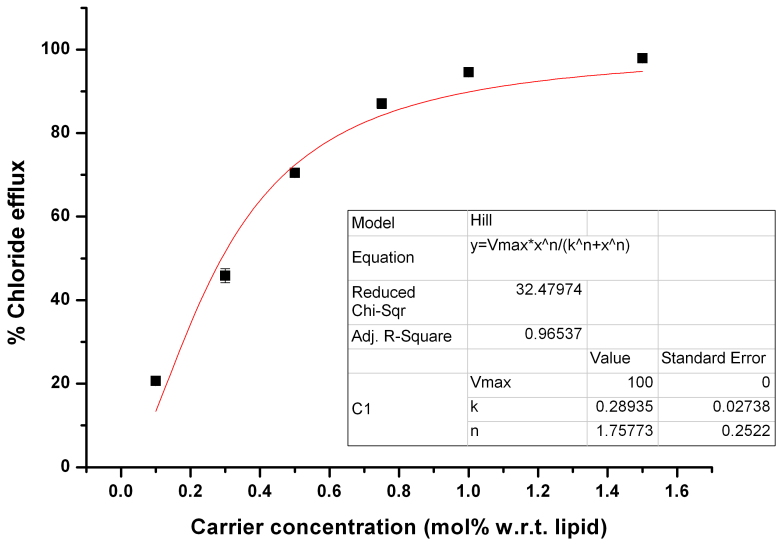

Fig. S43 Hill plot (repeat 3) for Cl^-/NO_3^- antiport by receptor **5**. $EC_{50,\,270\,s}$ = 0.29 mol%, *n* = 1.8.

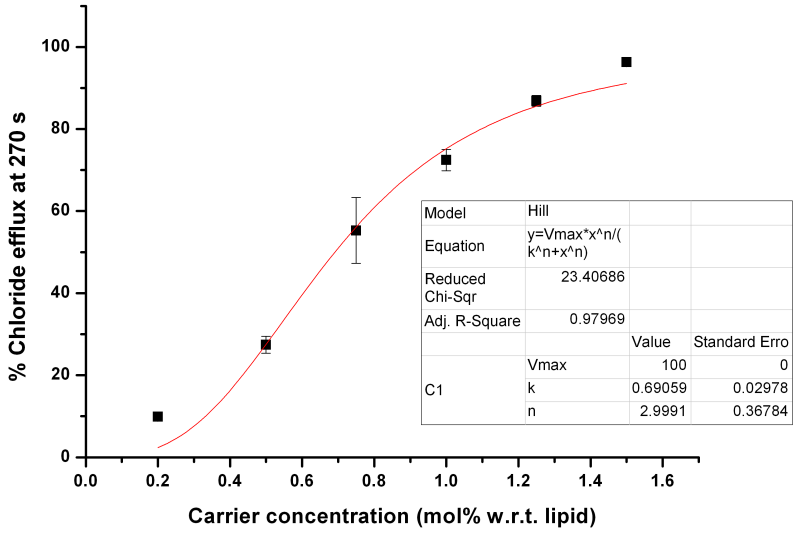

Fig. S44 Hill plot (repeat 1) for Cl^-/NO_3^- antiport by receptor **6**. $EC_{50,\ 270\ s}$ = 0.69 mol%, n = 3.0.

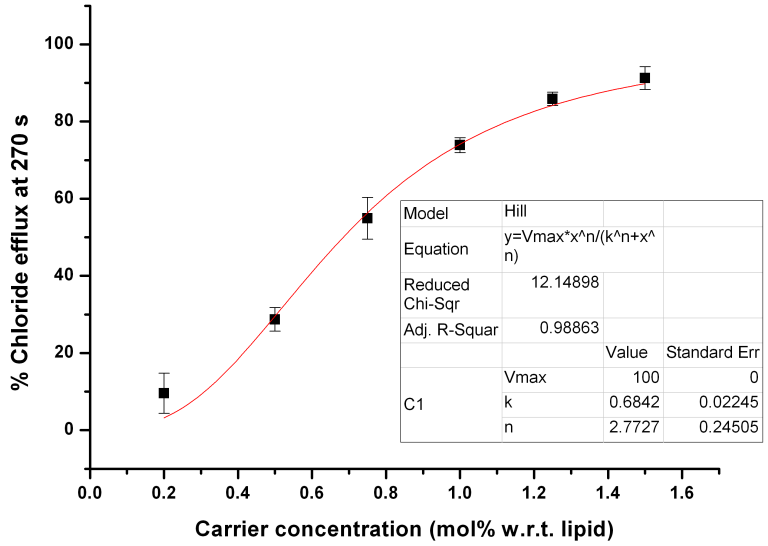

Fig. S45 Hill plot (repeat 2) for Cl^-/NO_3^- antiport by receptor **6**. $EC_{50,\ 270\ s}$ = 0.69 mol%, n = 2.8.

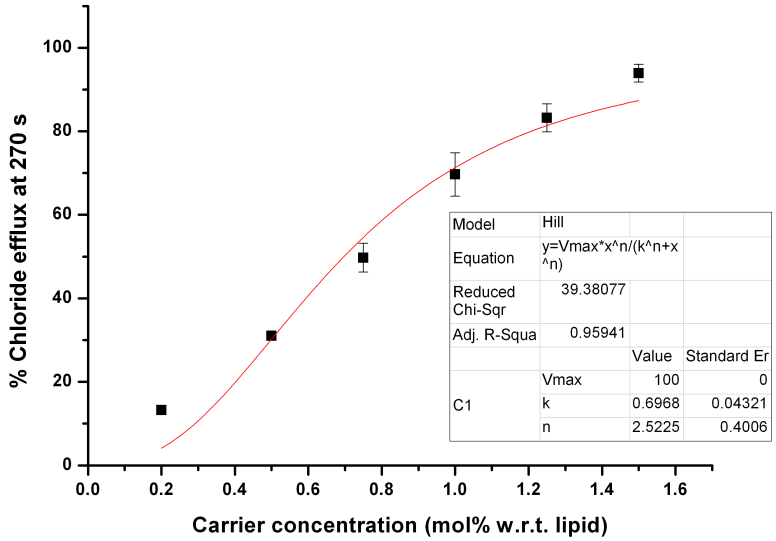

Fig. S46 Hill plot (repeat 3) for Cl^-/NO_3^- antiport by receptor **6**. $EC_{50,\ 270\ s}$ = 0.70 mol%, n = 2.5.

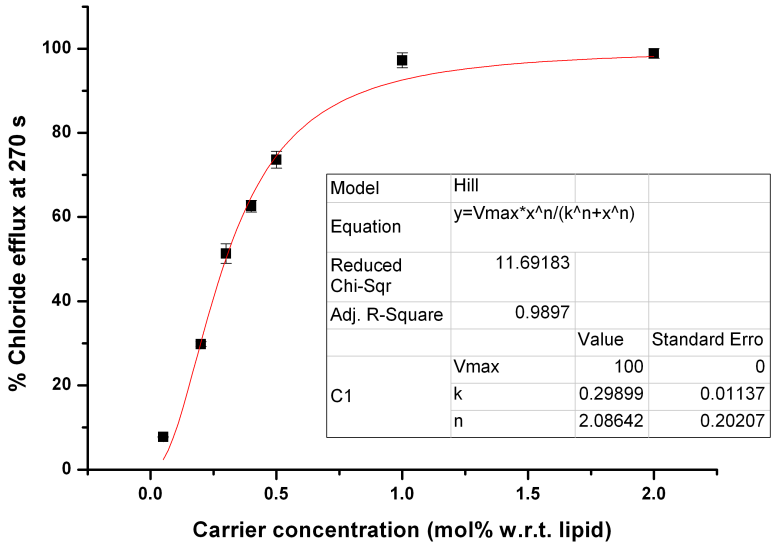

Fig. S47 Hill plot (repeat 1) for Cl^-/NO_3^- antiport by receptor **7**. $EC_{50,\ 270\ s}$ = 0.30 mol%, n = 2.1.

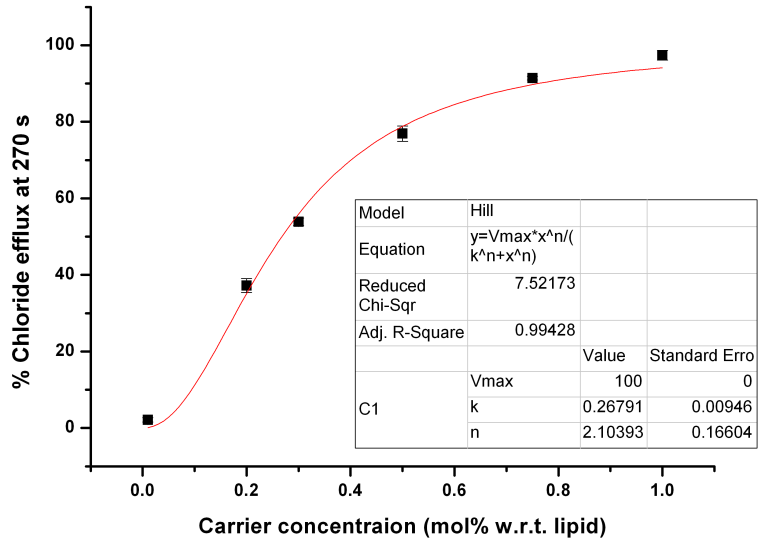

Fig. S48 Hill plot (repeat 2) for Cl^-/NO_3^- antiport by receptor **7**. $EC_{50,\ 270\ s}$ = 0.27 mol%, n = 2.1.

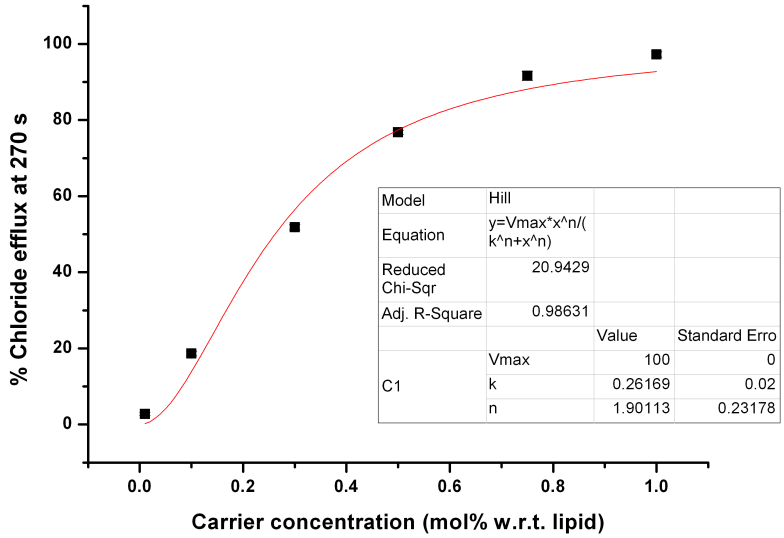

Fig. S49 Hill plot (repeat 3) for Cl^-/NO_3^- antiport by receptor **7**. $EC_{50,\ 270\ s}$ = 0.26 mol%, n = 1.9.

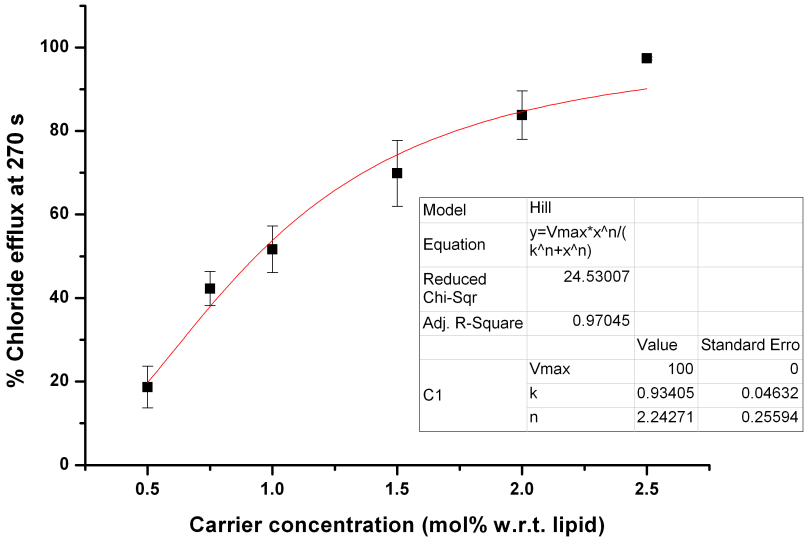

Fig. S50 Hill plot (repeat 1) for Cl^-/NO_3^- antiport by receptor **8**. $EC_{50,\ 270\ s}$ = 0.93 mol%, n = 2.2. NB All carrier concentrations were added using varying volumes of a 5 mM solution of the receptor in DMSO.

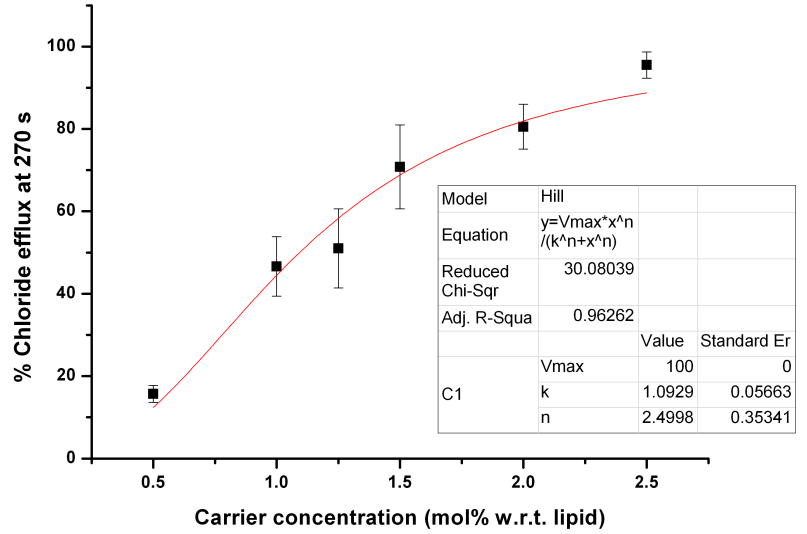

Fig. S51 Hill plot (repeat 2) for Cl^-/NO_3^- antiport by receptor **8**. $EC_{50,\ 270\ s}$ = 1.1 mol%, n = 2.5. NB All carrier concentrations were added using varying volumes of a 5 mM solution of the receptor in DMSO.

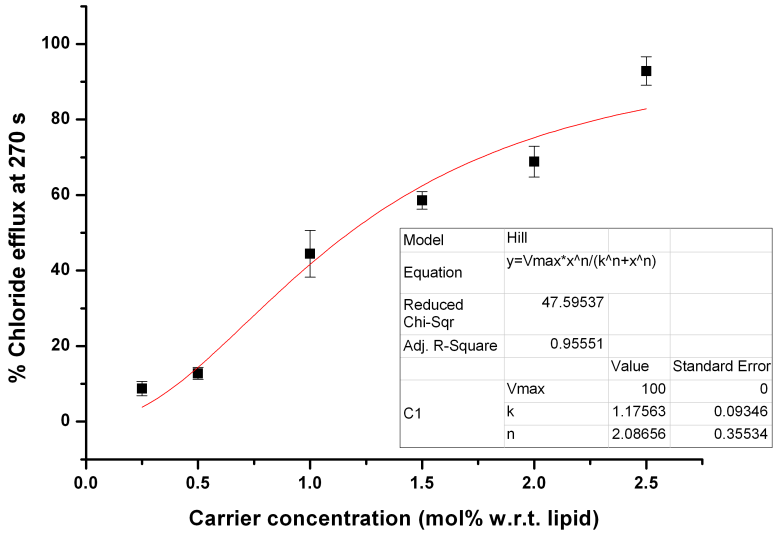

Fig. S52 Hill plot (repeat 3) for Cl^-/NO_3^- antiport by receptor **8**. $EC_{50,\ 270\ s}$ = 1.2 mol%, n = 2.1. NB All carrier concentrations were added using varying volumes of a 5 mM solution of the receptor in DMSO.

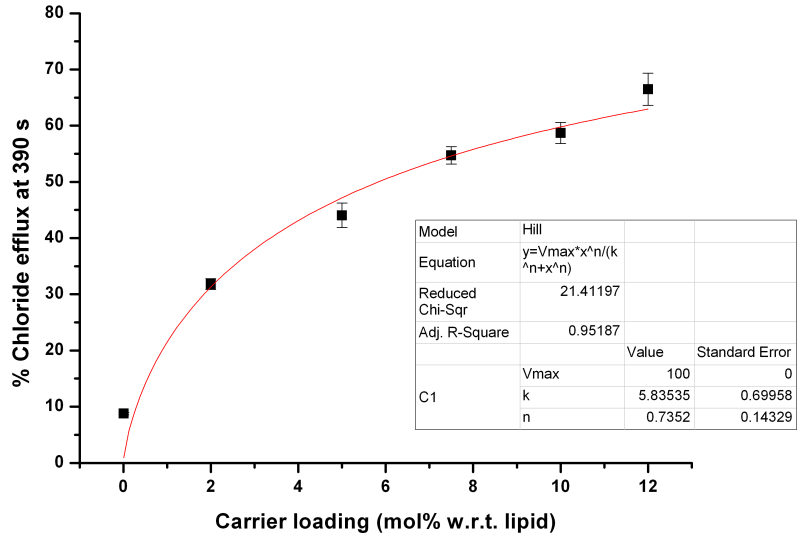

Fig. S53 Hill plot for Cl^-/HCO_3^- antiport by receptor **3**. $EC_{50,\ 390\ s}$ = 5.8 mol%, n = 0.73.

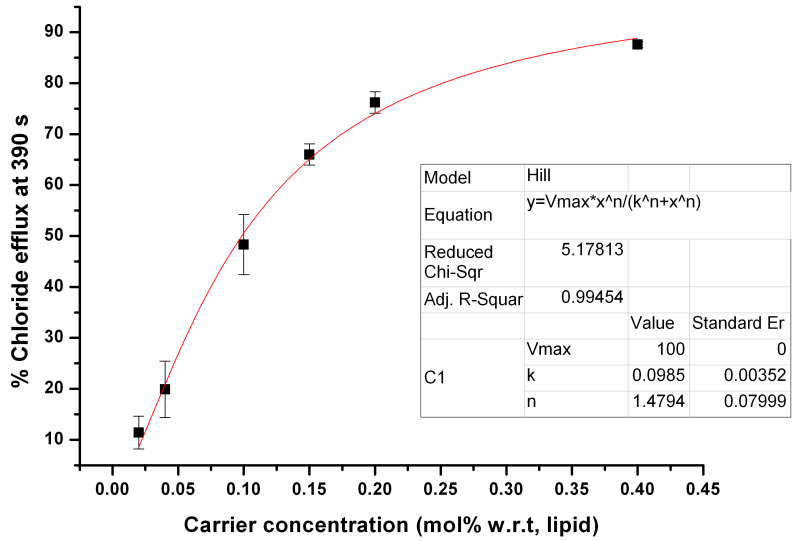

Fig. S54 Hill plot for Cl^-/HCO_3^- antiport by receptor **4**. $EC_{50,\ 390\ s}$ = 0.10 mol%, n = 1.5.

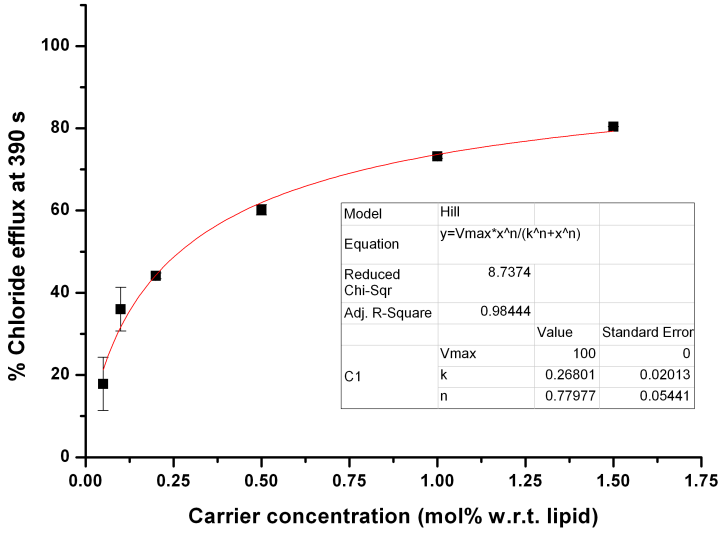

Fig. S55 Hill plot for Cl^-/HCO_3^- antiport by receptor **5**. $EC_{50,\ 390\ s}$ = 0.27 mol%, n = 0.78.

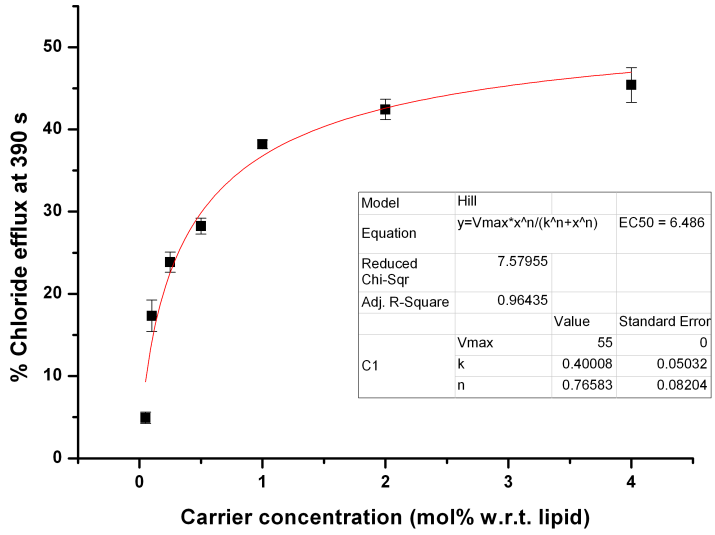

Fig. S56 Hill plot for Cl^-/HCO_3^- antiport by receptor **6**. V_{max} was fixed at 55 %. Calculated $EC_{50,\ 390\ s}$ = 8.1 mol%, n = 0.77.

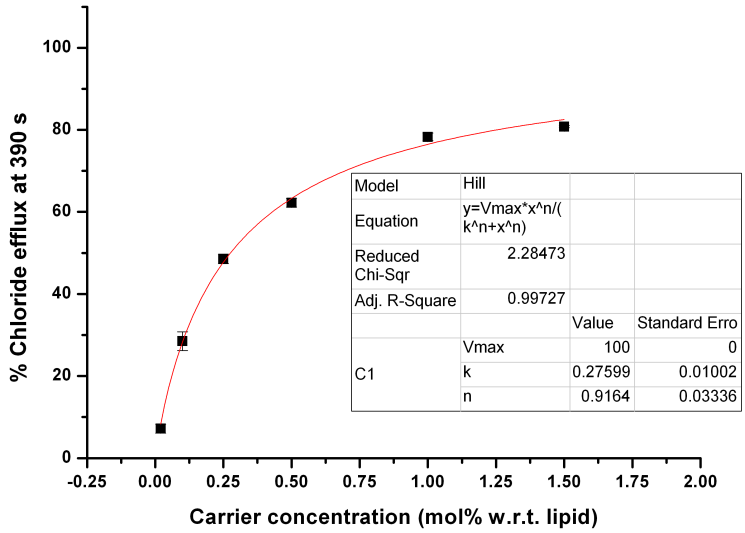

Fig. S57 Hill plot for Cl^-/HCO_3^- antiport by receptor **7**. $EC_{50,\ 390\ s}$ = 0.28 mol%, n = 0.91.

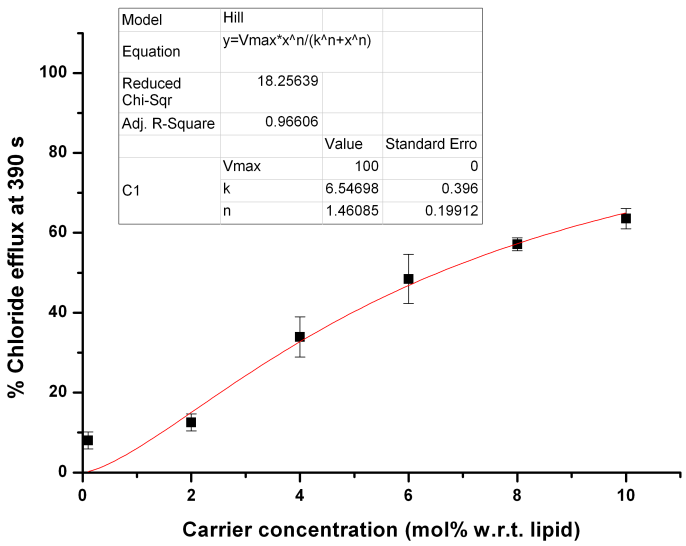

Fig. S58 Hill plot for Cl^-/HCO_3^- antiport by receptor **8**. $EC_{50,\ 390\ s}$ = 6.5 mol%, *n* = 1.46.

7.5 M^+/Cl^- symport assays

Unilamellar POPC vesicles containing NaCl or CsCl, prepared as described above, were suspended in 167 mM $NaNO_3$ buffered to pH 7.2 with sodium phosphate salts. The lipid concentration per sample was 1 mM. A DMSO solution of the carrier molecule (10 mM) was added to start the experiment and the chloride efflux was monitored using a chloride selective electrode. At 5 min, the vesicles were lysed with 50 µl of polyoxyethylene(8)lauryl ether (0.232 mM in 7:1 water:DMSO *v/v*) and a total chloride reading was taken at 7 min.

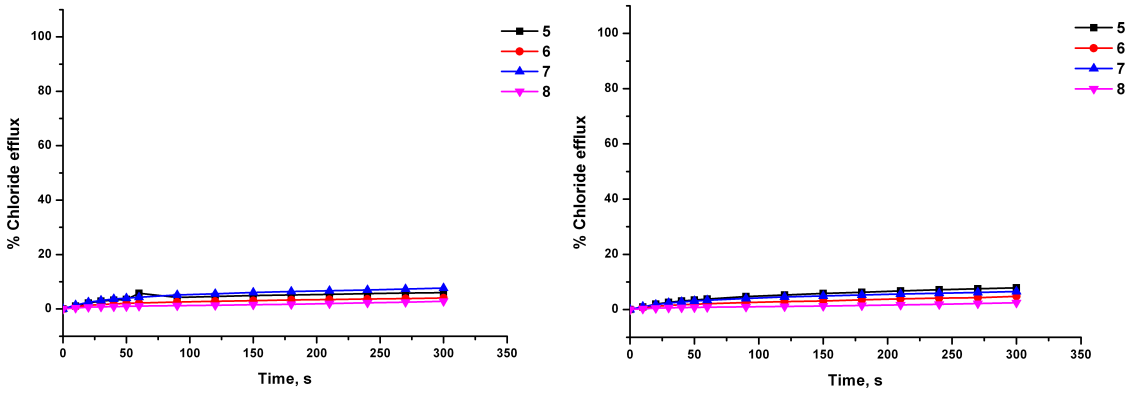

Fig. S59 Chloride release mediated by receptors **5-8** (2 mol% w.r.t. lipid) from POPC vesicles containing NaCl (left) or CsCl (right) suspended in Na_2SO_4.

7.6 Cholesterol assays

In order to probe the effect of modifying the membrane viscosity on anion transport activity, the Cl^-/NO_3^- antiport assay was repeated for receptors **5-8** in vesicles composed of POPC/cholesterol (7:3). The chloride efflux after 270 s in both POPC and POPC/cholesterol vesicles is shown below.

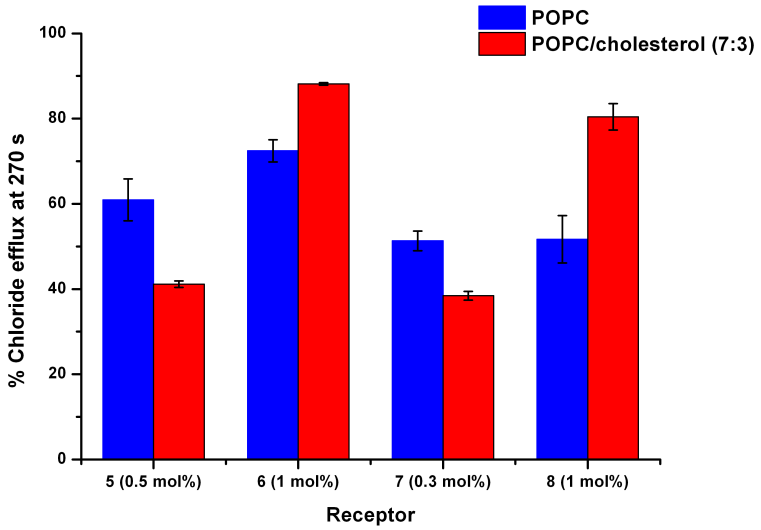

Fig. S60 Chloride efflux (Cl^-/NO_3^- antiport) mediated by receptors **5-8** from vesicles composed of POPC and POPC/cholesterol (7:3) in 270 s. Each point is the average of 3 trials (error bars represent the standard deviation).

7.7 U-tube experiments

Source phase: 489 mM NaCl buffered to pH 7.2 with 5 mM sodium phosphate salts, 10 mL.

Receiver phase: 489 mM NaNO3 buffered to pH 7.2 with 5 mM sodium phosphate salts, 10 mL.

Organic phase: 2 mM tetrabutylammonium hexafluorophosphate in nitrobenzene with 1 mM receptor **6** or **8** (no receptor was added for blank run), 20 mL.

The organic phase was stirred gently at room temperature, and the chloride concentration of the receiver phase was determined using a chloride sensitive electrode (Accumet) after 0 days, 2 days and 7 days.

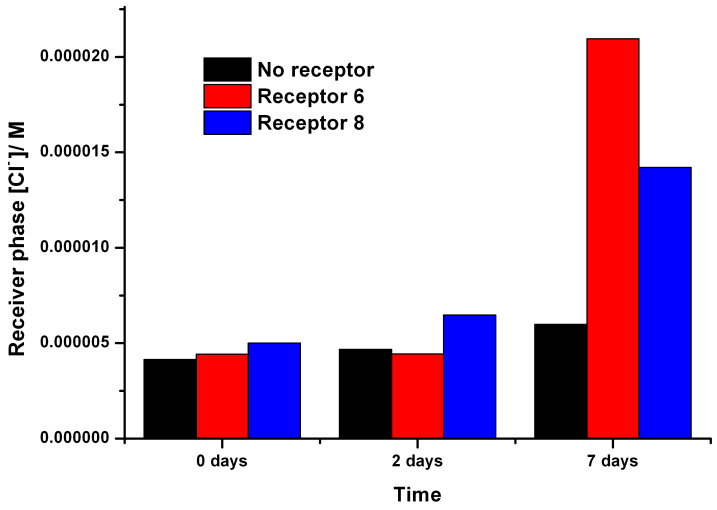

Fig. S61 The change in chloride concentration of the receiver phase of a U-tube apparatus mediated by receptors **6** and **8** (1 mM) compared to a control experiment with no receptor added.

8 Chloride ^{1}H NMR titration stack plots

NMR titrations were performed by addition of aliquots of the putative anionic guest as the tetrabutylammonium (0.15 M), in a solution of the receptor (0.01 M) in DMSO-d_6/0.5% H_2O, to a 0.01 M solution of the receptor in DMSO- $d_6$0.5% H_2O. Both salt and receptor were dried under high vacuum prior to use. ^{1}H NMR spectra were recorded on a Bruker AV300 or AV400 spectrometer and calibrated to the residual solvent peak in DMSO-d_6 (δ = 2.50 ppm).

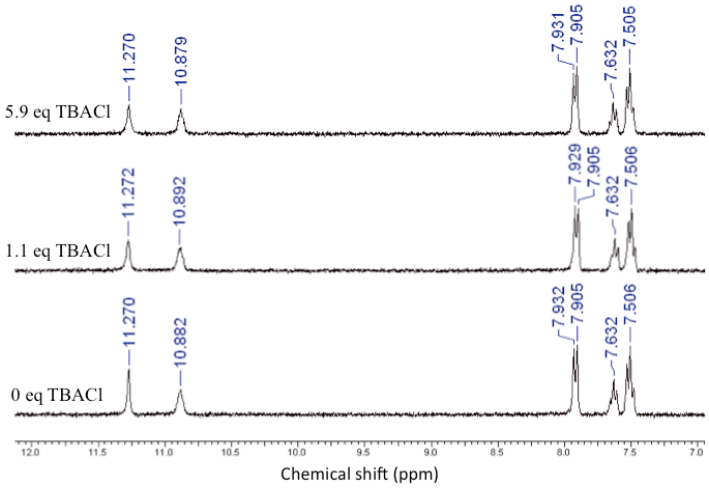

Fig. S62 Stack plot showing the titration of receptor **5** with tetrabutylammonium chloride in DMSO-d_6/ H_2O 0.5 % at 298 K.

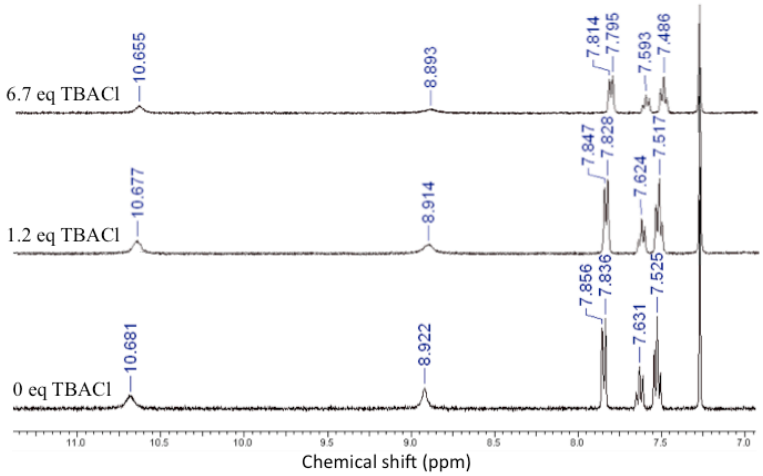

Fig. S63 Stack plot showing the titration of receptor **5** with tetrabutylammonium chloride in DMSO-d_6/ H_2O 0.5 % at 323 K.

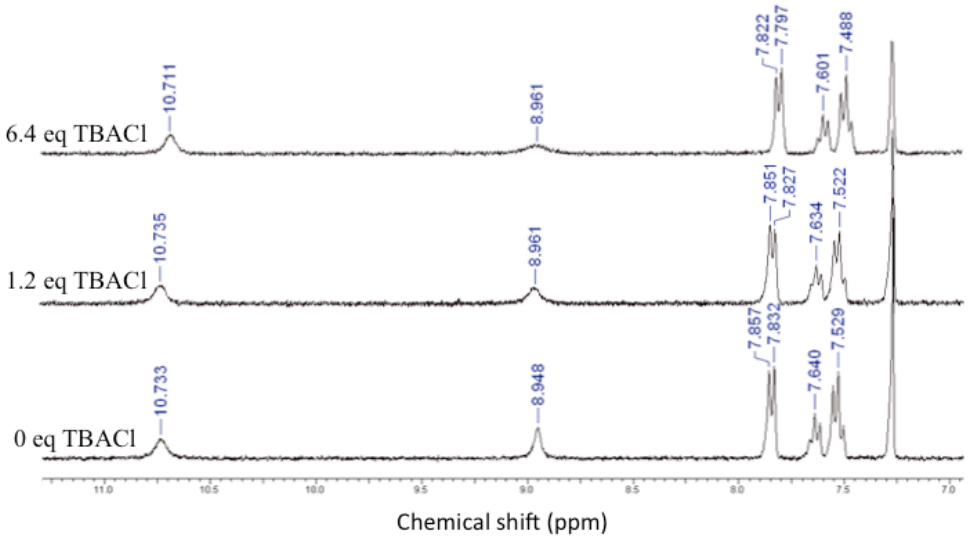

Fig. S64 Stack plot showing the titration of receptor **5** with tetrabutylammonium chloride in $CDCl_3$ at 298 K.

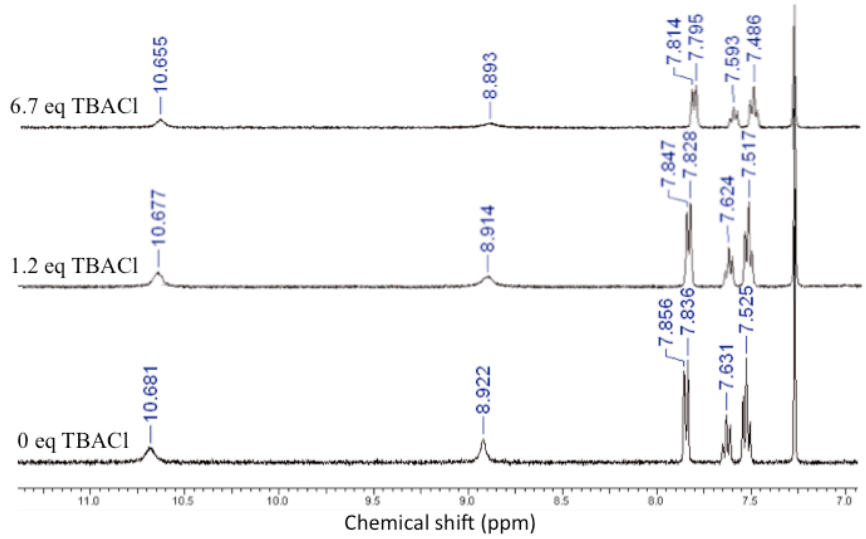

Fig. S65 Stack plot showing the titration of receptor **5** with tetrabutylammonium chloride in $CDCl_3$ at 323 K.

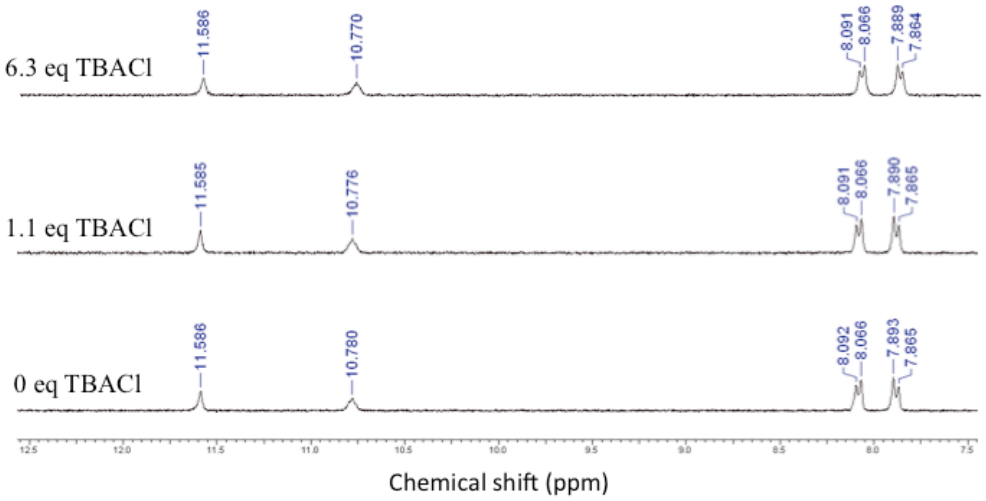

Fig. S66 Stack plot showing the titration of receptor **6** with tetrabutylammonium chloride in DMSO-d_6/ H_2O 0.5 % at 298 K.

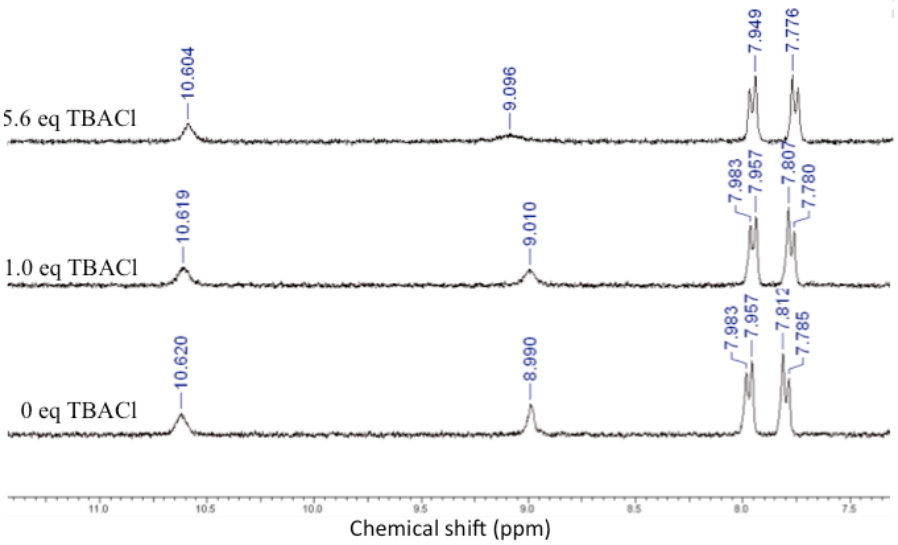

Fig. S67 Stack plot showing the titration of receptor **6** with tetrabutylammonium chloride in $CDCl_3$ at 298 K.

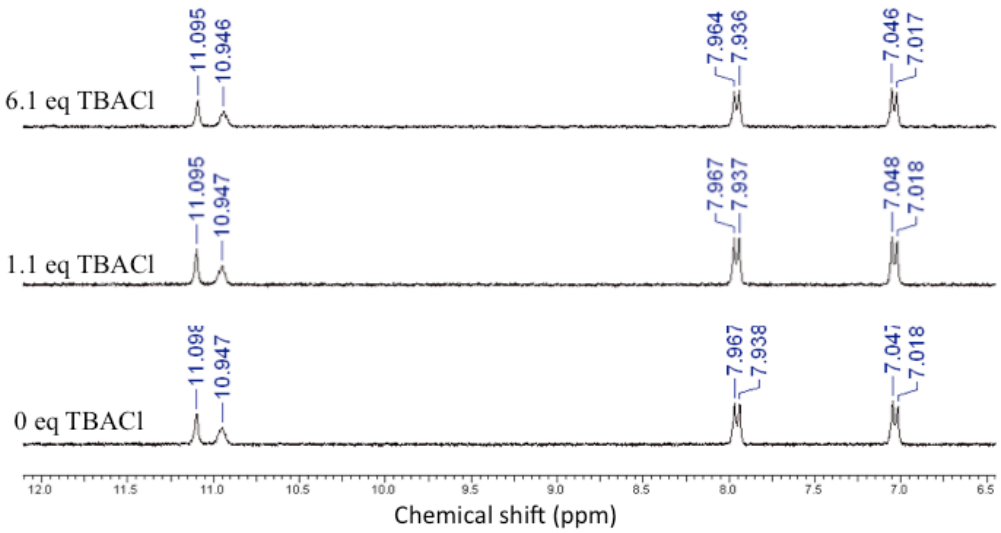

Fig. S68 Stack plot showing the titration of receptor **7** with tetrabutylammonium chloride in DMSO-d_6/ H_2O 0.5 % at 298 K.

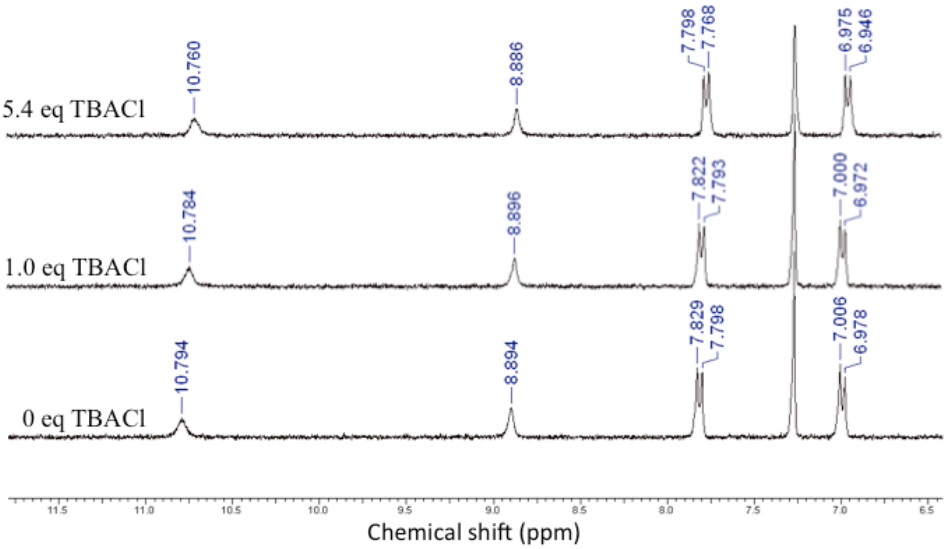

Fig. S69 Stack plot showing the titration of receptor **7** with tetrabutylammonium chloride in $CDCl_3$ at 298 K.

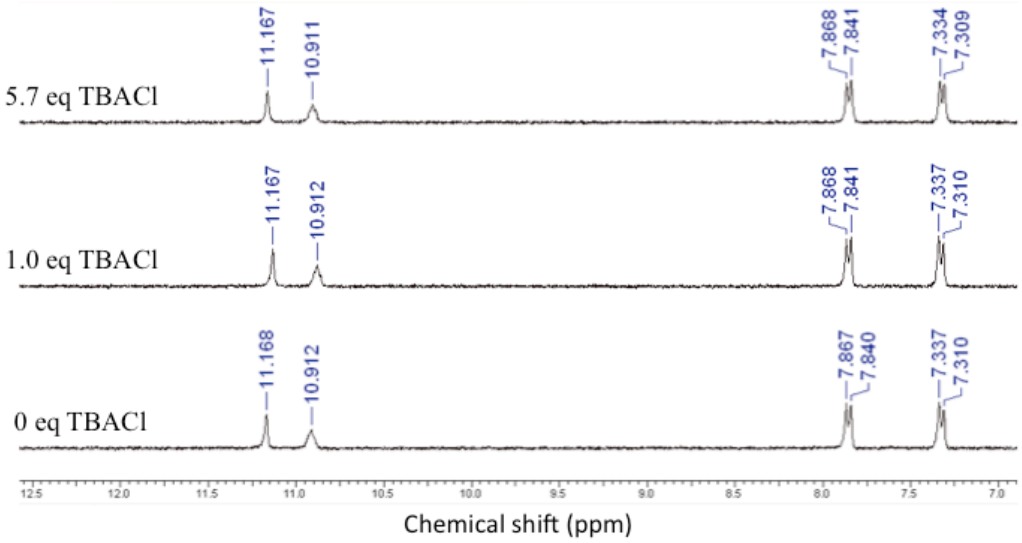

Fig. S70 Stack plot showing the titration of receptor **8** with tetrabutylammonium chloride in DMSO-d_6/ H_2O 0.5 % at 298 K.

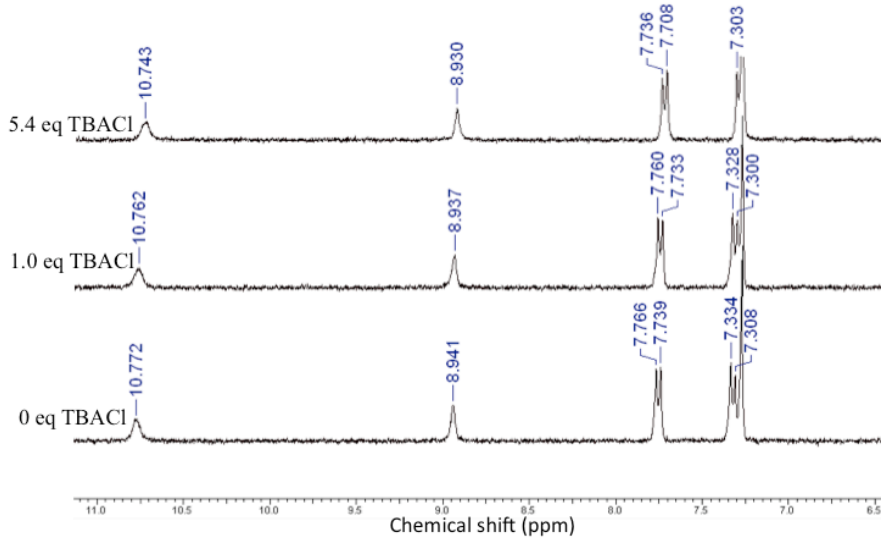

Fig. S71 Stack plot showing the titration of receptor **8** with tetrabutylammonium chloride in $CDCl_3$ at 298 K.

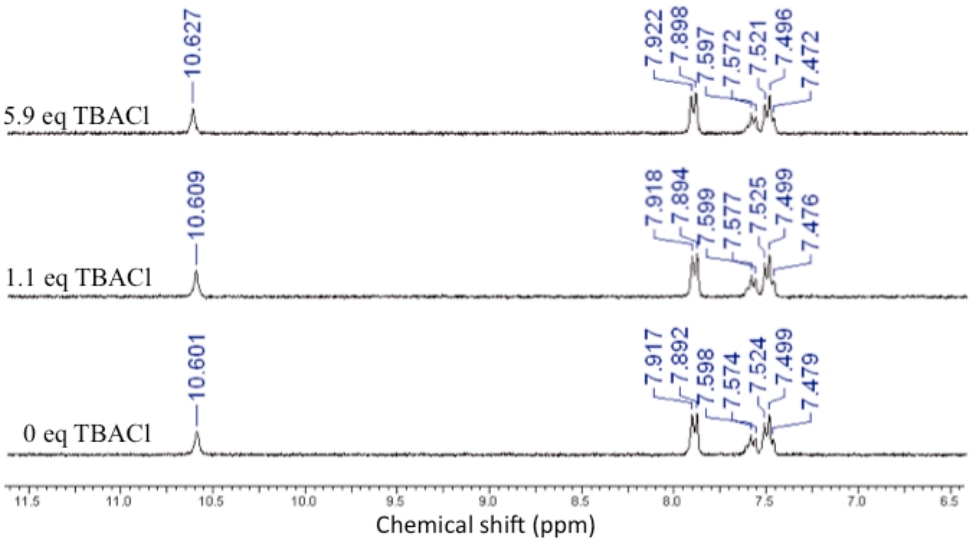

Fig. S72 Stack plot showing the titration of receptor **9** with tetrabutylammonium chloride in DMSO-d_6/ H_2O 0.5 % at 298 K.

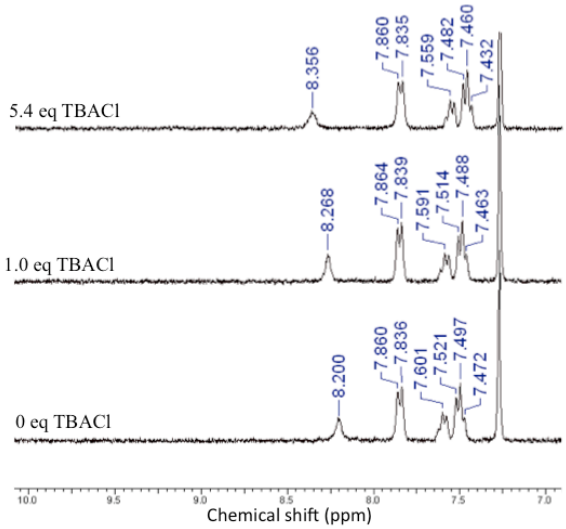

Fig. S73 Stack plot showing the titration of receptor **9** with tetrabutylammonium chloride in $CDCl_3$ at 298 K.

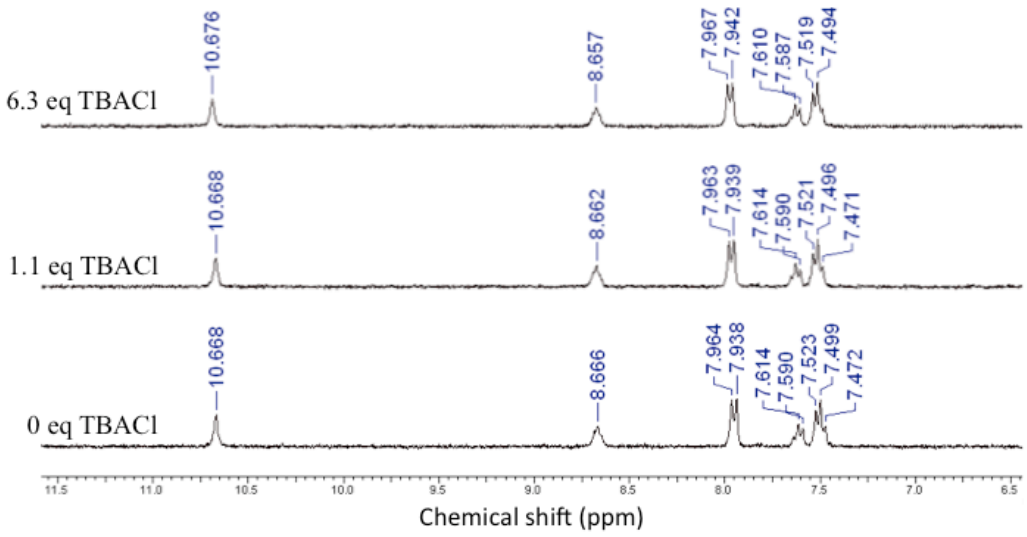

Fig. S74 Stack plot showing the titration of receptor **10** with tetrabutylammonium chloride in DMSO-d_6/ H_2O 0.5 % at 298 K.

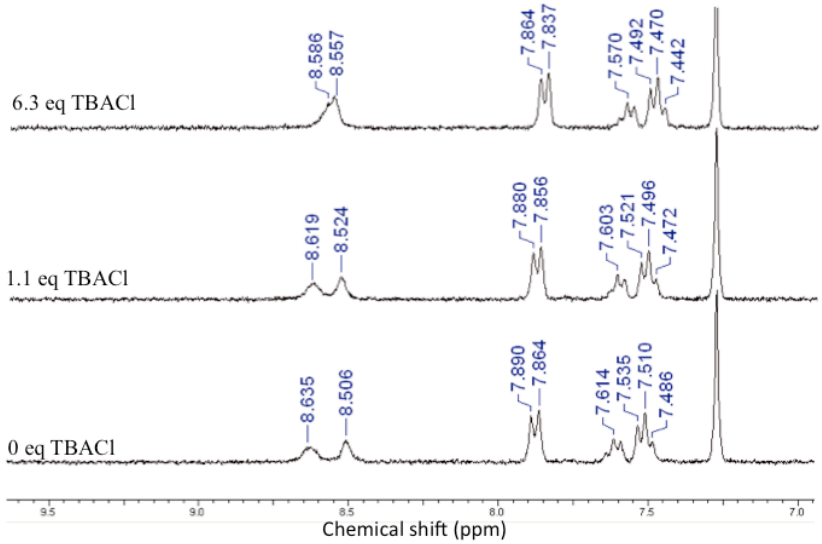

Fig. S75 Stack plot showing the titration of receptor **10** with tetrabutylammonium chloride in $CDCl_3$ at 298 K.

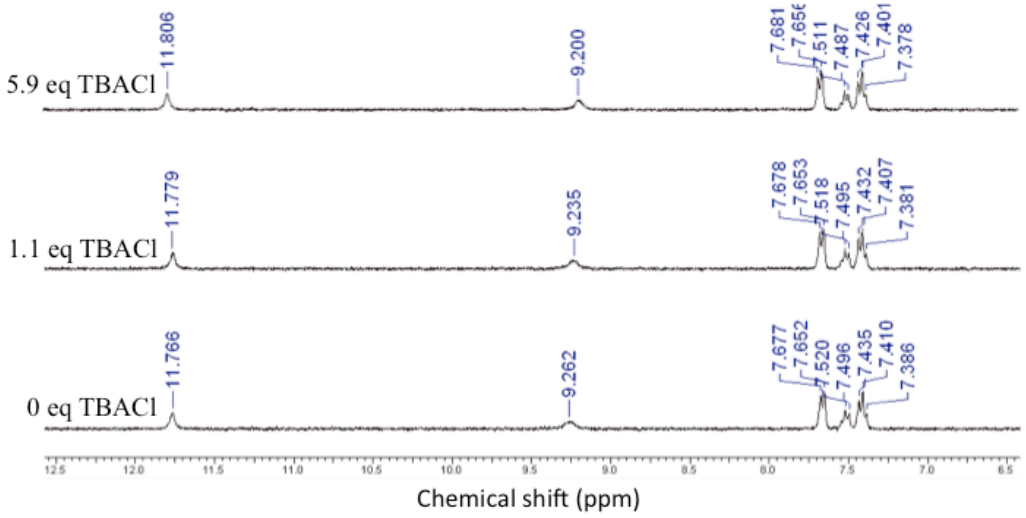

Fig. S76 Stack plot showing the titration of receptor **11** with tetrabutylammonium chloride in DMSO-d_6/ H_2O 0.5 % at 298 K.

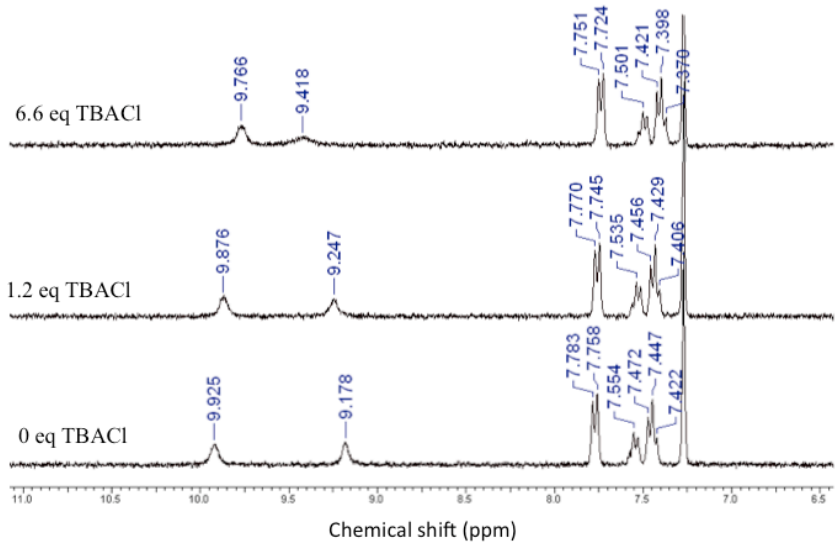

Fig. S77 Stack plot showing the titration of receptor **11** with tetrabutylammonium chloride in $CDCl_3$ at 298 K.

9 HPLC experiments

In order to assess the relative lipophilicity of the receptors studied, we utilised a previously reported HPLC experiment using a reverse phase column, as the retention time on the reverse phase column is related to its lipophilicity. The HPLC mobile phase was prepared with LC-MS grade methanol and water (Fisher Scientific UK, Loughborough, UK) containing 0.1% HCOOH each. Samples were prepared as a solution in LC-MS grade methanol at a concentration of 2 μg/mL. HPLC separations were performed on a Dionex Ultimate® 3000 UHPLC (Thermo Scientific, Hemel Hempstead, UK). Samples were injected (2 μL) directly onto a Kinetex C18 Column (50 mm X 2.1 mm 1.7 μm particle size; Phenomenex, Torrance, CA, USA) thermostatically controlled at 40°C. The separation was achieved using 50% methanol in water for 2 minutes followed by a linear gradient to 100% methanol over 12 minutes and returned to 50 % methanol for 2 minutes at a flow rate of 0.3 mL/min. UV data were recorded at 254 nm and mass spectra were recorded using a Maxis™ ESI-ToF mass spectrometer (Bruker Daltonics, Bremen, Germany) using positive ion electrospray ionisation (120-1500 *m/z*) in order to assign to retention time to the respective receptor.

The retention times of receptors **1**-**4** in a similar experiment have been previously reported. Good correlation was found between the previously reported values and those determined in this report (see below).

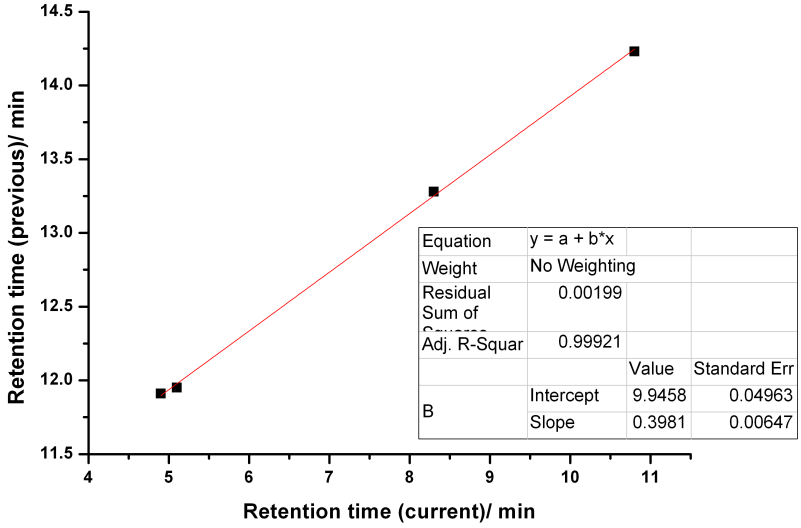

Fig. S78 Correlation between previously reported retention times for receptors **1**-**4** and those reported in this study